

# View-Consistent Diffusion Representations for 3D-Consistent Video Generation

Duolikun Danier<sup>1</sup> Ge Gao<sup>2</sup> Steven McDonagh<sup>1</sup> Changjian Li<sup>1</sup> Hakan Bilen<sup>1</sup> Oisin Mac Aodha<sup>1</sup>  
<sup>1</sup>University of Edinburgh <sup>2</sup> University of Bristol

## Abstract

Video generation models have made significant progress in generating realistic content, enabling applications in simulation, gaming, and film making. However, current generated videos still contain visual artifacts arising from 3D inconsistencies, e.g., objects and structures deforming under changes in camera pose, which can undermine user experience and simulation fidelity. Motivated by recent findings on representation alignment for diffusion models, we hypothesize that improving the multi-view consistency of video diffusion representations will yield more 3D-consistent video generation. Through detailed analysis on multiple recent camera-controlled video diffusion models we reveal strong correlations between 3D-consistent representations and videos. We also propose ViCoDR, a new approach for improving the 3D consistency of video models by learning multi-view consistent diffusion representations. We evaluate ViCoDR on camera controlled image-to-video, text-to-video, and multi-view generation models, demonstrating significant improvements in the 3D consistency of the generated videos. Project page: <https://danier97.github.io/ViCoDR>.

## 1. Introduction

The conditional generation of videos from inputs such as text [31], images [7], and camera trajectories [32, 71] offers the potential to transform applications such as world simulation for embodied AI [1, 108], gaming [15, 54], and movie production [57, 102]. Empowered by large-scale video datasets [5], advances in models [36, 70, 73], and training strategies [16, 60], diffusion-based video generation has made significant progress in generating realistic videos. However, recent studies [2, 103] have shown that these methods, trained solely to model the distribution of video frames, often fail to maintain 3D consistency, *i.e.*, ensuring all generated video frames are 2D projections of the same underlying 3D world. This results in physically implausible outputs [45, 58], where structures distort over time (see first row of Fig. 1), thereby reducing visual quality [120] and hindering 3D reconstruction [71, 78].

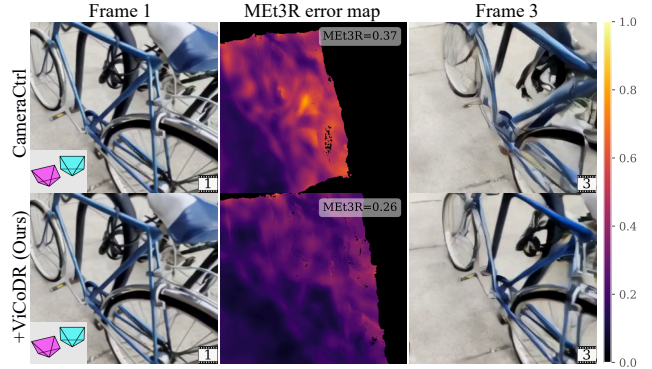


Figure 1. **Training video diffusion models (VDMs) with ViCoDR results in more 3D-consistent output videos.** ViCoDR enforces view-consistent diffusion representations during training, enhancing the VDMs’ 3D awareness. Here we show generated frames from a camera controlled VDM [32], where we see significant visual artifacts on the front wheel and frame of the bike. In contrast, ViCoDR’s output is more 3D consistent, as shown by the MET3R [2] reprojection error map.

To address this lack of 3D consistency, prior work has attempted to introduce additional 3D information obtained from off-the-shelf geometry estimation models to impose 3D-aware constraints, by providing the generative model with extra inputs as conditions during training and inference, including re-projected point clouds [71, 85], point maps represented as 3D coordinates [30], or combinations thereof [13]. However, these methods require the external geometric signals during inference, increasing computation, and are prone to errors when the employed geometric estimators are inaccurate. Other methods attempt to learn to jointly generate video pixels and the underlying geometry, using point maps [82, 115] or 3D Gaussians [78], but depend on paired high-quality 3D data for obtaining the training targets, which is expensive to collect at scale [100].

It has been shown that aligning diffusion representations with self-supervised vision encoders [68], known for strong semantic features [20], can enhance *image* generation quality [50, 111]. Inspired by this finding, recent works have extended such representation distillation to video generation [99, 117] or have additionally supervised video diffusion representations on auxiliary tasks [41, 45]. These

methods avoid the extra inference cost and requirement for 3D supervision, but do not provide a clear understanding of the underlying properties of diffusion representations that govern 3D consistency in video generation.

In contrast, multi-view-consistent visual *representations*, wherein features of the same 3D point remain consistent under view changes, have been shown to encode geometric knowledge [112] and benefit a range of tasks that require 3D understanding, including 3D reconstruction [64], pose estimation [61], depth estimation [112], and tracking [110]. This motivates our central question: *Does improving the view consistency of diffusion representations enhance the 3D consistency of the resulting generated videos?*

To address this question, we investigate camera-controlled video generation, where 3D consistency is crucial for realistic and geometrically coherent results [29, 78]. We conduct an empirical analysis on several recent video diffusion models, evaluating both their generation quality and the multi-view consistency of their internal representations. Our results demonstrate a strong correlation between these factors, highlighting the importance of view-consistent representations for high-quality output videos.

We also introduce ViCoDR, a new approach for 3D-consistent video diffusion via multi-view consistent diffusion representations. By incorporating a ranking-based correspondence loss that leverages geometric priors [92] to enforce view-invariant pixel representations to inject 3D awareness, we improve the 3D consistency of video generation. Unlike existing methods, ViCoDR adds no additional inference cost, and does not require high-quality 3D data for training. Compared to recent approaches [41, 45, 99] that also focus on enhancing diffusion representations, ViCoDR applies a more direct and effective constraint on view consistency, a key driver of 3D consistent generation. We apply ViCoDR to three categories of recent video diffusion models (VDMs): camera-controlled image-to-video [32], text-to-video [98], and multi-view generation [103], and observe consistent improvements.

To summarize, we make the following contributions:

- For the first time, we show that there is a strong correlation between the 3D consistency of the videos generated by multiple recent VDMs and the view consistency of their internal representations.
- We introduce ViCoDR, a new model-agnostic approach for enhancing 3D consistency in video generation by enforcing view consistent representations during training.
- We demonstrate substantial quantitative improvement in 3D consistency across three types of controllable VDMs.

## 2. Related Work

**Diffusion-based Video Generation.** Advancements in diffusion models [36, 46, 73] has led to a plethora of text/image-to-video (T/I2V) diffusion models. Early

works [7, 8, 17, 31, 34, 37, 95, 104, 118] extended image diffusion models to the temporal domain by training additional modules that capture inter-frame dependencies. Empowered by large-scale data [19, 67] and transformer architectures [25, 70], a new group of DiT-based video generators [10, 18, 48, 91, 109, 121] have shown impressive progress in generating high-resolution realistic videos, with more recent techniques focusing on long-term, auto-regressive generation [16, 21, 24, 42, 119]. In parallel, another major line of research focuses on controllability, *e.g.*, conditioning generation on text, image [58], audio [33], human pose [39], motion [98], and camera trajectory [32, 98, 107]. In this paper, we primarily focus on camera controlled generation, which closely relates to novel view synthesis [47, 65] where maintaining 3D consistency is of particular importance.

**3D-Consistent Camera Control.** Controlling the camera trajectory of generated videos enables novel view synthesis [78] and 3D scene generation [29]. While such control can be achieved with text descriptions [40, 53], explicitly conditioning on camera parameters [3, 4, 32, 49, 52, 98, 105, 107] has been shown to be a more effective alternative. However, recent studies [2, 103] have highlighted a persistent lack of 3D consistency in the outputs of these models. Existing approaches to address this issue can be broadly divided into two groups. The first enhances 3D awareness of the diffusion model by providing additional 3D-consistent conditioning. Specifically, some methods [38, 71] render the point cloud estimated from the input conditioning image into the desired views, and use these rendered views to condition the generation. Re-projection of point maps [94] (*i.e.*, pixel-aligned 3D coordinates) was similarly utilized in [30], and these ideas were combined in [13]. Limitations include computational overhead during inference, and reliance on external geometry estimation models, failure of which can lead to inaccurate outputs. The second group of methods jointly models the distribution of pixel values and underlying geometry. For example, paired RGB frames and point maps were generated in [82, 115], and [78] directly modeled 3D scene distributions (with 3D Gaussians [47]). Although these formulations achieve simultaneous generation and reconstruction, they are constrained by the limited availability of large-scale, high-quality 3D data. Compared to these approaches, our approach incurs no additional inference cost, and does not require explicit ground-truth 3D coordinate supervision for training.

**Diffusion Representations.** A number of works have studied the representations within diffusion models [3, 22, 41, 45, 63, 113], revealing their utility across various semantic and geometric tasks, *e.g.*, semantic correspondence [114], visual grounding [87], 4D reconstruction [62], and point tracking [45]. More recently, several works [50, 111] have studied the role of representation in generation itself, and

found that aligning diffusion representations to those in strong self-supervised vision encoder [68] is effective for enhancing image generation. Inspired by this, we explore enhancing 3D consistency of video generation by improving view consistency of video diffusion representations. Concurrent to our work, several methods [6, 44, 99, 117] have applied representation alignment on video generation, but these mostly focus on temporal coherence and physical plausibility of *object motion*, instead of 3D consistency. The closest works to ours are [41] and [99], which additionally supervise diffusion representations using pre-trained monocular 3D reconstruction models [92] via point map regression and feature distillation, respectively. However, it is not clear which properties of their diffusion representations are crucial for enforcing 3D consistency in the generated videos. In contrast, our novel analysis uncovers the importance of view-consistent diffusion representations for 3D-consistent video generation, and we take a more direct approach to inject 3D awareness by explicitly promoting this key property within VDMs. Our results demonstrate the superior performance of our approach over [41] and [99].

**View Consistent Representations.** View-consistent representations enable the establishment of geometric correspondence across views, which is essential for 3D understanding and reconstruction [72]. [27] showed that, despite highly-performant abilities in semantic and monocular geometric tasks, visual foundation models fall short on encoding multi-view correspondence. This observation has motivated a series of works [110, 112, 122] on improving the 3D awareness of these *image* models by learning view-consistent representations. We take inspiration from these works by enforcing view consistency in video diffusion representations during training.

### 3. Analyzing the 3D Consistency of VDMs

Recent studies suggest that enhancing the multi-view consistency of 2D visual representations improves their 3D awareness [112] and performance on tasks requiring accurate 3D perception [27, 61, 64, 112]. Building on this insight, we investigate the importance of view consistency of *video* diffusion representations for 3D-consistent video generation. To this end, we conduct an empirical analysis on seven VDMs, evaluating the 3D consistency of their generated videos (Task I), and the view consistency of their representations (Task II).

Our study focuses on camera-controlled video generation setting, where the goal is to generate novel views of a scene given a camera trajectory, hence the content in the scene are exposed to view changes. This setting underpins applications such as 3D reconstruction [82] and world generation [85], where the impact of 3D inconsistency is amplified. Therefore, it has been the main focus in recent 3D-consistent video generation research [2, 13, 71, 99, 115],

supported by established 3D consistency metrics [2, 26].

**Task I - Video Generation.** In camera-controlled image-to-video generation, the VDM is conditioned on an input image and a desired camera trajectory. The goal is to generate a video where the input image is the first frame, and the subsequent frames are consistent with the input camera trajectory. We run existing VDMs on the same dataset to obtain generated videos. To assess the 3D consistency of the generated videos, we use MEt3R [2], which measures pixel reprojection error in the feature space of visual foundation models [14, 28] across generated frames, and has been shown to accurately capture quality degradation due to 3D inconsistency.

**Task II - Geometric Correspondence.** To evaluate the view consistency of the *representations* within camera-controlled VDMs, we follow existing approaches [27, 84, 114] and use the keypoint-free correspondence estimation task [81], where pixel-level features extracted from a VDM are used to establish geometrically grounded pixel correspondences across different views of a scene via feature-space nearest-neighbor search. View-consistent representations encode the same 3D point in the generated scene more consistently across different viewpoints, hence leading to more accurate correspondences. Specifically, given a video and the corresponding camera trajectory, to extract diffusion features using a VDM, we add a small amount of noise [84] to the video (latents) and run a VDM forward pass. We obtain per-frame dense feature maps from the  $L$ th layer of the diffusion model, which are then bilinearly upsampled spatially (and temporally, if needed) to obtain the pixel-wise features for evaluating geometric correspondence. Results are reported in terms of pixel-space correspondence recall, measured as the percentage of detected pixel correspondences with Euclidean distance below a threshold. See Appendix for more details.

**Dataset.** To evaluate video generation, we selected RealEstate10K (RE10K) [123] and DL3DV [55]. To control for the impact of data distribution in our analysis, we use the same datasets for evaluating geometric correspondence. Specifically, to obtain 2D correspondences across frames, we pseudo-label the test videos using an efficient state-of-the-art feed-forward geometric estimation model, VGGT [92]. These labels are imperfect, but are of sufficient quality for our analysis. See Appendix for more details.

**Models.** We evaluated seven different camera-controlled image-to-video models: CameraCtrl [32], MotionCtrl[98], GEN3C [71], GWTF [12], DaS [30], MVGenMaster [13], and RealCamI2V [52]. To perform inference, we follow the original setup of each model as described in their official documentation. Full details are provided in the Appendix.

**Results.** In Fig. 2 it can be observed that the 3D consistency of generated videos (MEt3R) strongly correlates with the view consistency of VDM representations. This is also

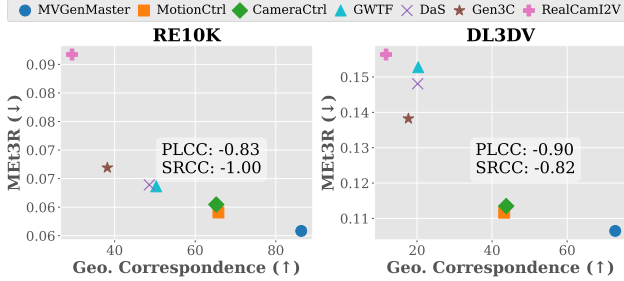


Figure 2. **Analysis of 3D consistency in camera-controlled VDMs.** We observe a strong correlation between 3D consistency of video generation (measured by MET3R) and view consistency of VDM representations (measured by geometric correspondence).

evident in terms of both Pearson’s linear correlation (PLCC) and Spearman’s rank correlation coefficients (SRCC). That is, models whose internal representations are more view-consistent (indicating stronger “3D awareness”) tend to produce more 3D-consistent videos. Our analysis is not specific to a model type, as the evaluated models vary in both their architectures and training data. This finding provides a possible explanation for the reason behind the effectiveness of recent attempts to improve 3D consistency in video generation by supervising diffusion representations using feature distillation [99] and 3D reconstruction [41], both of which encourage view-consistent representations [22, 88] indirectly. While our results do not imply a causal relationship, they provide strong empirical motivation for the design of our method, ViCoDR, where we incorporate an additional supervision signal to directly encourage the learning of view-consistent representations during VDM training to improve their 3D consistency.

## 4. ViCoDR

Our analysis in Sec. 3 uncovered a strong correlation between 3D consistency in video generation and view-consistent representations. Motivated by this, we propose ViCoDR, a new method to improve 3D consistency by explicitly enforcing multi-view-consistent diffusion representations. The core idea is to employ an additional loss during VDM training to encourage the learning of view-invariance in the internal representations of the same 3D points. Fig. 3 provides an overview of our approach. First, we review video diffusion briefly, then introduce the overall pipeline of ViCoDR, and present details of our view consistency loss.

### 4.1. Preliminaries: Video Diffusion Models (VDMs)

A VDM  $f_\theta$ , parameterized by  $\theta$ , aims to learn the distribution  $p(x^{1:N}|\mathcal{C})$  of  $N$  video frames  $x^{1:N}$  with some conditioning  $\mathcal{C}$ , typically in a compact latent space [73] of a

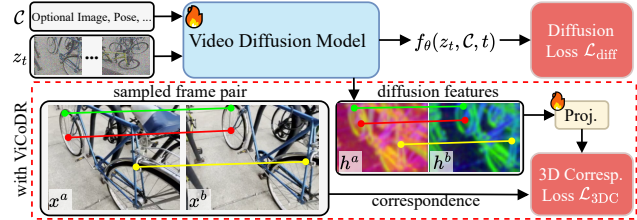


Figure 3. **Overview of ViCoDR.** During video diffusion training, ViCoDR additionally supervises internal diffusion representations ( $h^a, h^b$ ) extracted from frame pairs ( $x^a, x^b$ ) with a 3D correspondence loss (Eq. (5)), so as to learn view-consistent representations (PCA feature maps are visualized).

pre-trained VAE  $\{\mathcal{E}, \mathcal{D}\}$ , with the objective:

$$\mathcal{L}_{\text{diff}} = \mathbb{E}_{z_0, \mathcal{C}, \epsilon, t} [\|y - f_\theta(z_t, \mathcal{C}, t)\|_2^2], \quad (1)$$

where  $z_0 = \mathcal{E}(x^{1:N})$ , and  $z_t$  are the noisy video latents corrupted by random Gaussian noise  $\epsilon \sim \mathcal{N}(0, I)$  at diffusion timestep  $t$  following a schedule [36, 46]. The prediction target  $y$  can be computed from  $\epsilon$  and/or  $z_0$  using different parameterizations [36, 56, 75, 80], e.g.,  $y = \epsilon$  in a noise-prediction setting. The diffusion network  $f_\theta$  can be implemented as a U-Net [74] equipped with temporal modules or a DiT [70]. During inference, the VDM iteratively denoises the latents  $z_t$ , initialized as random Gaussian noise at  $t = T$ , and the generated video is then obtained by decoding the clean latents  $x^{1:N} = \mathcal{D}(z_0)$ .

### 4.2. Overall Pipeline

Recent works [2, 45, 103, 115] have shown that VDMs trained on the diffusion loss (Eq. (1)) alone often fail to produce 3D-consistent videos, resulting in objects and rigid structures deforming over time. A possible reason is that by solely learning the distribution of 2D pixels, which are essentially lossy projections of the 3D world, these models struggle to encode that the pixel transformations can often be easily explained by the underlying scene geometry and SE(3) transforms [66, 99] and this lack of “3D awareness” could be improved via learning view-consistent representations [27, 110, 112].

In addition to the standard diffusion loss (Eq. (1)), we enforce additional supervision on the intermediate representations of  $f_\theta$  to promote view consistency. Specifically, we first extract per-frame feature maps  $h^{1:N} \in \mathbb{R}^{N \times H_{\text{ft}} \times W_{\text{ft}} \times C}$  from noisy video latents at the  $L$ th layer of  $f_\theta$ :

$$h^{1:N} = f_\theta^L(z_t^{1:N}, \mathcal{C}, t), \quad (2)$$

where  $H_{\text{ft}}, W_{\text{ft}}$ , and  $C$  denote the spatial size and channel dimensions of the features. These features are then passed to a convolutional projector network  $g_\phi$  before being bilingually up-sampled to obtain image-resolution features  $\tilde{h}^{1:N} \in \mathbb{R}^{N \times H \times W \times C} = \text{Up}[g_\phi(h^{1:N})]$ . The additional view consistency loss  $\mathcal{L}_{3DC}$  (described in Sec. 4.3) is

then calculated using these projected features, with the corresponding gradients back-propagated into  $f_\theta$  up to layer  $L$ . To allow 3D-consistent features  $\tilde{h}^{1:N}$  to more directly influence the generation process, we use the approach from [45] and pass  $\tilde{h}^{1:N}$  back to the diffusion network through a zero-initialized linear layer  $r_\varphi$ , updating the original features after detaching the gradient:

$$h^{1:N} := h^{1:N} + r_\varphi(\text{StopGrad}[\tilde{h}^{1:N}]). \quad (3)$$

Detaching the gradient ensures that the features  $\tilde{h}^{1:N}$  are not directly influenced by the diffusion loss, hence it can focus primarily on learning view consistency [45].

During VDM training, our method simply adds an additional loss term to form the combined loss:

$$\mathcal{L}_{\text{total}}(\{\theta, \phi, \varphi\}) = \mathcal{L}_{\text{diff}} + \lambda \mathcal{L}_{3\text{DC}}, \quad (4)$$

where the parameters of the additional modules  $g_\phi, r_\varphi$  are trained together with the VDM (these modules are not used during inference). Here  $\lambda$  is a hyperparameter weighting the view consistency term, and we study its impact in Sec. 5.4. Next, we present the details of  $\mathcal{L}_{3\text{DC}}$ .

### 4.3. View Consistency Loss

To learn view-consistent representations, we assume a static scene, and employ a ranking-based 3D correspondence loss [110]. Specifically, having computed  $\tilde{h}^{1:N}$ , we randomly sample a pair of frames  $(x^a, x^b)$  and their corresponding features  $(\tilde{h}^a, \tilde{h}^b)$ , normalizing the latter to get  $(\bar{h}^a, \bar{h}^b)$  for cosine-similarity calculation later. From each frame, we sample  $K$  pixel locations as keypoints, and, assuming access to their 3D coordinates, we calculate their pair-wise 3D Euclidean distance in order to find pixel correspondences. Treating each keypoint from frame  $x^a$  as a query point  $q$ , we retrieve for each  $q$  a positive sample keypoint  $p$  from frame  $x^b$  that has the smallest distance to it, discarding queries whose distance to its positive sample is above a threshold  $t_{\text{pos}}$  (indicating failed correspondence matching). For each valid query, we also sample a negative set  $\mathcal{S}_n$  containing keypoints in frame  $x^b$  with 3D distance to  $q$  above  $t_{\text{neg}}$ , whose features are used as negative samples in the loss. Then, the 3D correspondence loss for each query  $q$  is computed as  $\mathcal{L}_{3\text{DC}}^q =$

$$1 - \frac{1}{|\mathcal{S}_p|} \sum_{i \in \mathcal{S}_p} \frac{1 + \sum_{j \in \mathcal{S}_p, j \neq i} \sigma_\tau(D_{ij}^q)}{1 + \sum_{j \in \mathcal{S}_p, j \neq i} \sigma_\tau(D_{ij}^q) + \sum_{j \in \mathcal{S}_n} \sigma_\tau(D_{ij}^q)}, \quad (5)$$

where  $\sigma_\tau(\cdot)$  is a sigmoid function with a constant temperature  $\tau = 0.01$ ,  $\mathcal{S}_p = \{q, p\}$  is the set of positive samples (including  $q$  itself), and  $D_{ij}^q = \bar{h}_q \cdot \bar{h}_j - \bar{h}_q \cdot \bar{h}_i$  is the difference in feature cosine similarity of samples to point  $q$ . The losses for all queries are then aggregated to obtain  $\mathcal{L}_{3\text{DC}} = \frac{1}{|\mathcal{Q}|} \sum_{q \in \mathcal{Q}} \mathcal{L}_{3\text{DC}}^q$ , where  $\mathcal{Q}$  denotes all eligible queries.

This is a ranking-based loss originally used for image retrieval in [11]. The second term in Eq. (5) represents smooth average precision, a differentiable approximation of average precision, which measures the rank (in terms of similarity to  $q$ ) of a positive sample among all positive samples (the numerator) over its rank among all samples (the denominator). The loss essentially encourages query features to have higher similarity to positive samples (*i.e.*, the same 3D points) compared to negative samples (*i.e.*, distant points), and has been shown effective for learning correspondence in [110]. ViCoDR only trains with this additional loss, and does not incur any extra inference-time computational cost.

**Pseudo 3D labels.** Commonly used datasets for training video generation models (*e.g.*, RE10K [123] or DL3DV [55] for camera-controlled generation) do not come with densely annotated 3D points. While it is possible to obtain 3D points by running optimization-based reconstruction methods [69, 76, 77], considering efficiency and reconstruction density, we choose to make use of strong geometric priors learned from large-scale pre-trained models. Specifically, we employ VGGT [92], a state-of-the-art feed-forward 3D reconstruction network, to label pixel values with their corresponding 3D coordinates. Due to its ranking-based nature,  $\mathcal{L}_{3\text{DC}}$  imposes a constraint on *relative* feature similarity rather than on their absolute values. This is a less strict objective than feature distillation [92] or point map regression [41], hence is more robust than these methods to imperfections in the pseudo labels, as supported by our experiments (Sec. 5.2).

**Edge-aware sampling.** Due to memory constraints, the number of keypoints  $K$  sampled during training cannot span all possible points. To overcome this, during training we bias the sampling of keypoints on image edges detected with a Sobel filter. This emphasizes 3D consistency at object boundaries and textural details. We show empirically in Sec. 5.4 that this further improves the 3D consistency of the generated videos compared to uniform random sampling.

## 5. Experiments

### 5.1. Setup

To validate the effectiveness of ViCoDR, we experiment with different video diffusion models, re-training them with their original training data and configurations using (i) their original losses only, and (ii) combined with our consistency loss  $\mathcal{L}_{3\text{DC}}$ , for the same number of iterations.

**Base models.** As discussed in Sec. 3, we mainly focus on the camera-controlled I2V setting, where the goal is to generate novel views of a scene following a user-provided input image and camera trajectory. For this, we choose CameraCtrl (ver. SVD) [32] as our base model, which is a representative recent approach that is computationally feasible to re-train. Furthermore, to show the effectiveness of

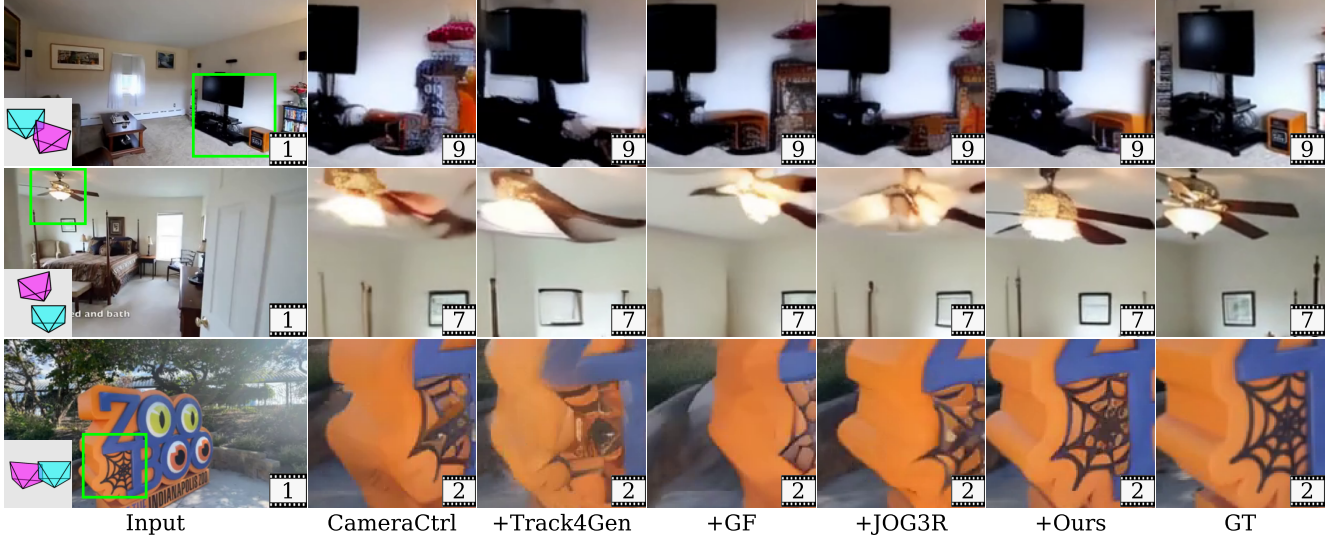


Figure 4. **Qualitative comparison with baseline methods on CameraCtrl.** CameraCtrl trained with ViCoDR is able to generate more 3D-consistent video frames at new viewpoints compared to the baselines. Frame indices are shown at the bottom right of each image. The first column indicates the conditioning input, where at the bottom left we illustrate the camera poses of the **input frame** and the plotted **novel view**. The first two rows show examples from RE10K, and the last row from DL3DV. See examples in the supplementary video.

Table 1. **Comparison with baseline methods on CameraCtrl.** Training with ViCoDR results in largest increase in **3D consistency** compared to other baseline approaches. The **MEt3R** score of CameraCtrl is improved by 11% on RE10K and 8% on DL3DV, while its **RPE** performance boosted by 13% on RE10K and 11% on DL3DV. ViCoDR also maintains competitive performance in terms of both image/video quality metrics (PSNR, SSIM, LPIPS, FVD) and camera control accuracy (RotErr, TransErr, Success rate).

RE10K									
Model	PSNR ( $\uparrow$ )	SSIM ( $\uparrow$ )	LPIPS ( $\downarrow$ )	FVD ( $\downarrow$ )	RotErr ( $\downarrow$ )	TransErr ( $\downarrow$ )	Succ % ( $\uparrow$ )	MEt3R ( $\downarrow$ )	RPE ( $\downarrow$ )
CameraCtrl	16.888	0.695	0.273	113	0.795	2.313	86.3	0.066	0.385
+Track4Gen	16.211	0.666	0.300	132	0.852	2.861	88.7	0.072	0.398
+GF	16.845	0.693	0.278	117	0.721	2.234	90.0	0.067	0.381
+JOG3R	16.103	0.670	0.296	120	0.913	2.702	86.7	0.066	0.375
+ViCoDR (ours)	<b>17.043</b>	<b>0.699</b>	<b>0.266</b>	<b>115</b>	<b>0.605</b>	<b>1.883</b>	<b>92.3</b>	<b>0.059</b>	<b>0.334</b>
DL3DV									
Model	PSNR ( $\uparrow$ )	SSIM ( $\uparrow$ )	LPIPS ( $\downarrow$ )	FVD ( $\downarrow$ )	RotErr ( $\downarrow$ )	TransErr ( $\downarrow$ )	Succ % ( $\uparrow$ )	MEt3R ( $\downarrow$ )	RPE ( $\downarrow$ )
CameraCtrl	13.318	0.493	0.433	113	2.119	4.619	63.4	0.120	0.662
+Track4Gen	12.965	0.478	0.479	227	2.600	5.610	54.9	0.137	0.689
+GF	13.185	0.491	0.447	124	2.425	5.449	54.6	0.132	0.735
+JOG3R	12.971	0.479	0.450	142	2.217	4.345	<b>69.5</b>	0.113	0.611
+ViCoDR (ours)	<b>13.467</b>	<b>0.499</b>	<b>0.431</b>	<b>119</b>	<b>2.023</b>	<b>4.144</b>	<b>69.1</b>	<b>0.110</b>	<b>0.586</b>

ViCoDR beyond CameraCtrl, we also experiment with a camera-controlled T2V model MotionCtrl (ver. AnimateDiff) [98], and a multi-view generation model ViFiGen [103].

**Implementation details.** When training ViCoDR, at each iteration  $\mathcal{L}_{3DC}$  is enabled only if the sampled noise level is within the first 20% of the noising schedule, similar to [41]. We set  $\lambda = 0.2, 0.7, 0.2$  for CameraCtrl, MotionCtrl, and ViFiGen respectively based on validation performance, and the number of keypoints to  $K = 20,000$ . Following [45], we set  $L$  to the second last layer for each base model. The projector network  $g_\phi$  is an eight layer convolutional network. We train each base model with their official training configurations, meaning the same optimization parame-

ters, trained modules, and training iterations, except for the ViCoDR version where we apply our additional loss term. However, due to computational constraints, we could not align with original batch sizes, and use the maximum possible with our setup for each model (see Appendix).

**Datasets.** During training, we use the original training datasets of each model: RE10K [123] for CameraCtrl and MotionCtrl, and Objaverse [23] for ViFiGen. If required, we use the text captions from [32]. For evaluation, we use a held-out test set of RE10K (300 videos), and a 1K subset of DL3DV [55], which contains more challenging scenes and trajectories. Following [90], we use a subset of OmniObj3D [101] for evaluating multi-view generation.

Table 2. **Results of ViCoDR on text-to-video generation.** ViCoDR improves MotionCtrl in terms of **video quality**, **camera control**, and **3D consistency** metrics. Mean over three seeds are reported on RE10K. Full results are included in the Appendix.

Model	FVD (↓)	RotErr (↓)	TransErr (↓)	Succ % (↑)	MEt3R (↓)	RPE (↓)
MotionCtrl	780	<b>1.119</b>	<b>4.676</b>	89.1	0.075	0.306
+ ViCoDR	<b>559</b>	1.217	5.288	<b>96.4</b>	<b>0.059</b>	<b>0.255</b>



Figure 5. **Qualitative results of applying ViCoDR to text-to-video generation.** Text prompt is shown above images. Arrows highlight 3D consistent/inconsistent regions. Better viewed zoomed-in. See more examples in the Appendix.

**Baselines.** We compare to existing SoTA approaches that attempt to improve the 3D awareness of VDMs. These include Track4Gen [45] and JOG3R [41], which train a VDM while also learning to track points and predict 3D point maps respectively. We also compare to the concurrent Geometry Forcing (GF) [99], which attempts to improve VDM representations by aligning them to VGGT features. We use the official implementation of GF to re-train the base VDM, and implement Track4Gen and JOG3R following the descriptions in the original papers as there is no code available at the time of writing.

**Evaluation metrics.** We evaluate camera-controlled generation using three criteria: image/video quality, camera controllability, and 3D consistency. For image/video quality we report PSNR, SSIM [97], LPIPS [116] and FVD [89] as in [71]. Following [32, 52], we evaluate camera controllability using Rotation (RotErr) and Translation (TransErr) Errors, which compares the camera poses from the generated video, reconstructed using COLMAP [76], to the input camera trajectory. The reconstruction success rate (Succ %) is also reported. We evaluate the 3D consistency of generated videos using MEt3R [2] and Reprojection Error (RPE) [26]. Finally, for the multi-view generation task, we follow MVGBench [103] and fit two 3D Gaussian Splatting (3DGS) models to disjoint subsets of generated views. Chamfer Distance (CD) and rendered depth error (Depth) are computed between the reconstructions to evaluate geometric consistency, while cPSNR, cSSIM, and cLPIPS are calculated between their rendered images and are used to assess the multi-view texture consistency. Full evaluation methodology details are provided in the Appendix.

## 5.2. Comparison to baselines

Here we validate the effectiveness of ViCoDR on a popular camera-controlled I2V model, CameraCtrl [32], and com-

Table 3. **Results of ViCoDR on multi-view generation.** Here on OmniObject3D, ViCoDR effectively improves multi-view generation in terms of 3D geometry and 3D texture consistency metrics.

Model	CD (↓)	Depth (↓)	cPSNR (↑)	cSSIM (↑)	cLPIPS (↓)
ViFiGen	2.98	11.66	28.91	0.92	<b>0.04</b>
+ ViCoDR	<b>2.97</b>	<b>11.59</b>	<b>29.03</b>	<b>0.94</b>	0.05



Figure 6. **Qualitative results on multi-view generation.** Our method maintains consistent geometry and appearance.

pare against baseline methods also designed for improving 3D consistency of video generation. Tab. 1 summarizes the quantitative results. We observe that, with the same number of training steps, training with ViCoDR results in the best overall performance on both RE10K and DL3DV. In particular, our method brings significant improvement in 3D consistency, enhancing the MEt3R and RPE score of CameraCtrl by 11% and 13% respectively on RE10K. The 3D consistency improvements are also evident on DL3DV, with an 8% and 11% increase for MEt3R and RPE. These improvements come with competitive performance on other image/video quality metrics (*i.e.*, PSNR, SSIM, LPIPS, FVD), and camera control accuracy (*i.e.*, PSNR, SSIM, LPIPS, Success rate), indicating the effectiveness of ViCoDR.

These quantitative results are further supported by the qualitative results in Fig. 4, where ViCoDR generates novel scene views with the least geometric deformation, while still respecting the conditioning camera poses. In line with our goal of improving 3D consistency, ViCoDR provides a clear quantitative and qualitative improvement over CameraCtrl, though some artifacts still remain, which are partially also tied to the inherent limitations of the base model.

The JOG3R and GF baselines also improve CameraCtrl in terms of 3D consistency metrics MEt3R and RPE, but perform worse than us. As discussed in Sec. 4.3, JOG3R supervises diffusion features to regress point maps directly, thus can be sensitive to imperfections in the pseudo labels from VGGT. GF enforces feature similarity between the VDM and VGGT, which may impose an overly strict constraint. In comparison, ViCoDR uses a ranking-based loss which makes it more robust to errors in VGGT, and directly promotes view consistency, a key property for 3D-consistent generation (Sec. 3). Track4Gen underperforms, which is likely because it derives its point tracking training targets from 2D optical flow [86], which can provide noisy supervision when chained to obtain longer-term tracklets.

### 5.3. Additional tasks

We further validate the effectiveness of ViCoDR by applying it to two other VDMs: MotionCtrl (ver. AnimateDiff, camera-controlled T2V) [98] and ViFiGen [103] (multi-view generation). MotionCtrl takes a text caption and camera trajectory as input (*i.e.*, with no image input), and aims to generate a video faithful to those inputs. ViFiGen takes an image of an object as input, and generates a multi-view set of images capturing the object at fixed target views. Due to its T2V nature (*i.e.*, scene content is only specified with text), there is a large variability in videos generated by MotionCtrl, so we run inference on MotionCtrl three times using different seeds.

For MotionCtrl, Tab. 2 shows that, compared to the default setting, training with ViCoDR largely improves FVD and 3D consistency (both MEt3R and RPE). However, a slight decrease in camera control performance is noticed, and this trade-off is discussed further in Sec. 5.4. Fig. 5 shows two visual examples where the structures are found better preserved when trained with our method.

For the multi-view generation task, ViCoDR notably enhances ViFiGen in both geometric and appearance consistency across viewpoints, as demonstrated quantitatively by the lower CD and Depth errors and higher cPSNR and cSSIM scores in Tab. 3. Visually, Fig. 6 shows that ViCoDR produces reconstructions with stronger multi-view structural and textural coherence, even (and particularly) in partially occluded regions, suggesting that the enforced cross-view consistency effectively stabilizes geometry and appearance across viewpoints.

### 5.4. Ablation study

Here we analyze the impact of our view consistency loss  $\mathcal{L}_{3DC}$  and ablate major design components on RE10K.

**Weight of  $\mathcal{L}_{3DC}$ .** We first study the impact of our view consistency loss by training CameraCtrl+ViCoDR with different values of  $\lambda$  (see Eq. (4)). Note, all models here (including CameraCtrl) are trained for the same number of iterations. The detailed results of these variants are shown in the Appendix. There we observe that all tested values of  $\lambda$  result in large improvements to the base model in terms of MEt3R, validating the effectiveness of our method. As  $\lambda$  increases, there is a very small improving trend in MEt3R, while the camera control errors (RotErr and TransErr) increase steadily (*e.g.*, RotErr increases from 0.605 to 0.743 on RE10K as  $\lambda$  increases from 0.2 to 1, and similarly for TransErr). This implies that ViCoDR leads to a trade-off between precise camera control and 3D-consistent video generation, though the overall performance still improves over the baseline CameraCtrl.

**Edge-aware Sampling.** Here we train ViCoDR (w/o edge) by disabling the bias towards sampling keypoints on edges (see Sec. 4.3). Tab. 4 shows that removing this step leads to a performance decrease, indicating the importance of our

Table 4. **Ablation results on RE10K.** “+Ours” is our default setup using VGGT. Performance degrades without edge-aware sampling. Using DUST3R is worse than VGGT but still brings improvements on 3D consistency.

Model	FVD (↓)	RotErr (↓)	TransErr (↓)	Succ % (↑)	MEt3R (↓)	RPE (↓)
CameraCtrl	113	0.795	2.313	86.3	0.066	0.385
+Ours	115	0.605	1.883	92.3	0.059	0.334
+Ours (w/o edge)	118	0.618	1.966	92.0	0.061	0.350
+Ours (DUST3R)	117	0.627	2.012	90.3	0.060	0.341

sampling strategy. See Appendix for qualitative results.

**Reliance on VGGT.** We investigate ViCoDR’s reliance on the quality of the pseudo correspondence labels used for the calculation of  $\mathcal{L}_{3DC}$ . Specifically, we train using DUST3R [94] instead of VGGT (Ours (DUST3R)), a similar feed-forward 3D reconstruction model that underperforms VGGT on a number of benchmarks [92]. The results in Tab. 4 show that while ViCoDR benefits from higher-quality labels, the performance degradation (especially in terms of 3D consistency) is not significant.

### 5.5. Limitations

Our experiments focus primarily on the camera-controlled setting. Therefore, similar to existing camera controlled VDMs [32, 52, 71], we train and evaluate on static scenes that do not feature dynamic objects. Training with ViCoDR requires some additional computation and GPU memory (more discussion on this in the Appendix). The models on which ViCoDR is applied are based on SVD [7] (CameraCtrl), AnimateDiff [31] (MotionCtrl), and SV3D [90] (ViFiGen). These models are moderately sized and generate low-resolution (*i.e.*, lower than 720p), short (1-2 seconds) videos [96], which can be limited in performance compared to larger models [43], which ultimately bounds the effectiveness of ViCoDR. Future work could explore integrating ViCoDR with larger-scale video generators [109] and autoregressive models [79].

## 6. Conclusion

We explored the role of multi-view consistent diffusion representations in 3D-consistent video generation. Through an empirical analysis on seven recent camera-controlled image-to-video diffusion models, we uncovered a correlation between view consistency of diffusion representations and 3D consistency of generated videos. Motivated by this, we proposed ViCoDR, a new approach for 3D-consistent video generation by enforcing view-consistent diffusion representations. We demonstrated the effectiveness of ViCoDR in improving 3D consistent video generation on three types of video models, reporting improvements over recent methods. We hope our work contributes to advancing 3D-consistent video generation to unlock its capabilities in immersive and safety-critical applications.

**Acknowledgments.** Funding was provided by ELIAI (the Edinburgh Laboratory for Integrated Artificial Intelligence) - EPSRC (EP/W002876/1).

## References

- [1] Niket Agarwal, Arslan Ali, Maciej Bala, Yogesh Balaji, Erik Barker, Tiffany Cai, Prithvijit Chattopadhyay, Yongxin Chen, Yin Cui, Yifan Ding, et al. Cosmos world foundation model platform for physical ai. *arXiv:2501.03575*, 2025. 1
- [2] Mohammad Asim, Christopher Wewer, Thomas Wimmer, Bernt Schiele, and Jan Eric Lenssen. Met3r: Measuring multi-view consistency in generated images. In *CVPR*, 2025. 1, 2, 3, 4, 7, 16, 18
- [3] Sherwin Bahmani, Ivan Skorokhodov, Guocheng Qian, Aliaksandr Siarohin, Willi Menapace, Andrea Tagliasacchi, David B Lindell, and Sergey Tulyakov. Ac3d: Analyzing and improving 3d camera control in video diffusion transformers. In *CVPR*, 2025. 2
- [4] Sherwin Bahmani, Ivan Skorokhodov, Aliaksandr Siarohin, Willi Menapace, Guocheng Qian, Michael Vasilkovsky, Hsin-Ying Lee, Chaoyang Wang, Jiaxu Zou, Andrea Tagliasacchi, et al. Vd3d: Taming large video diffusion transformers for 3d camera control. *ICLR*, 2025. 2
- [5] Max Bain, Arsha Nagrani, Gül Varol, and Andrew Zisserman. Frozen in time: A joint video and image encoder for end-to-end retrieval. In *ICCV*, 2021. 1
- [6] Aritra Bhowmik, Denis Korzhenkov, Cees GM Snoek, Amirhossein Habibi, and Mohsen Ghafoorian. Moalign: Motion-centric representation alignment for video diffusion models. *arXiv:2510.19022*, 2025. 3
- [7] Andreas Blattmann, Tim Dockhorn, Sumith Kulal, Daniel Mendelevitch, Maciej Kilian, Dominik Lorenz, Yam Levi, Zion English, Vikram Voleti, Adam Letts, et al. Stable video diffusion: Scaling latent video diffusion models to large datasets. *arXiv:2311.15127*, 2023. 1, 2, 8, 16, 17
- [8] Andreas Blattmann, Robin Rombach, Huan Ling, Tim Dockhorn, Seung Wook Kim, Sanja Fidler, and Karsten Kreis. Align your latents: High-resolution video synthesis with latent diffusion models. In *CVPR*, 2023. 2
- [9] Aleksei Bochkovskii, Amaël Delaunoy, Hugo Germain, Marcel Santos, Yichao Zhou, Stephan R Richter, and Vladlen Koltun. Depth pro: Sharp monocular metric depth in less than a second. *ICLR*, 2025. 17
- [10] Tim Brooks, Bill Peebles, Connor Holmes, Will DePue, Yufei Guo, Li Jing, David Schnurr, Joe Taylor, Troy Luhman, Eric Luhman, et al. Video generation models as world simulators. *OpenAI Blog*, 2024. 2
- [11] Andrew Brown, Weidi Xie, Vicky Kalogeiton, and Andrew Zisserman. Smooth-ap: Smoothing the path towards large-scale image retrieval. In *ECCV*, 2020. 5
- [12] Ryan Burgert, Yuancheng Xu, Wenqi Xian, Oliver Pilarski, Pascal Clausen, Mingming He, Li Ma, Yitong Deng, Lingxiao Li, Mohsen Mousavi, et al. Go-with-the-flow: Motion-controllable video diffusion models using real-time warped noise. In *CVPR*, 2025. 3, 17
- [13] Chenjie Cao, Chaohui Yu, Shang Liu, Fan Wang, Xiangyang Xue, and Yanwei Fu. Mvgenmaster: Scaling multi-view generation from any image via 3d priors enhanced diffusion model. In *CVPR*, 2025. 1, 2, 3, 17
- [14] Mathilde Caron, Hugo Touvron, Ishan Misra, Hervé Jégou, Julien Mairal, Piotr Bojanowski, and Armand Joulin. Emerging properties in self-supervised vision transformers. In *ICCV*, 2021. 3
- [15] Haoxuan Che, Xuanhua He, Quande Liu, Cheng Jin, and Hao Chen. Gamegen-x: Interactive open-world game video generation. *ICLR*, 2025. 1
- [16] Boyuan Chen, Diego Martí Monsó, Yilun Du, Max Simchowitz, Russ Tedrake, and Vincent Sitzmann. Diffusion forcing: Next-token prediction meets full-sequence diffusion. *NeurIPS*, 2024. 1, 2
- [17] Haoxin Chen, Menghan Xia, Yingqing He, Yong Zhang, Xiaodong Cun, Shaoshu Yang, Jinbo Xing, Yaofang Liu, Qifeng Chen, Xintao Wang, et al. Videocrafter1: Open diffusion models for high-quality video generation. *arXiv:2310.19512*, 2023. 2
- [18] Shoufa Chen, Chongjian Ge, Yuqi Zhang, Yida Zhang, Fengda Zhu, Hao Yang, Hongxiang Hao, Hui Wu, Zhichao Lai, Yifei Hu, et al. Goku: Flow based video generative foundation models. In *CVPR*, 2025. 2
- [19] Tsai-Shien Chen, Aliaksandr Siarohin, Willi Menapace, Ekaterina Deyneka, Hsiang-wei Chao, Byung Eun Jeon, Yuwei Fang, Hsin-Ying Lee, Jian Ren, Ming-Hsuan Yang, et al. Panda-70m: Captioning 70m videos with multiple cross-modality teachers. In *CVPR*, 2024. 2
- [20] Xuweiyi Chen, Markus Marks, and Zezhou Cheng. Probing the mid-level vision capabilities of self-supervised learning. In *CVPR*, 2025. 1
- [21] Justin Cui, Jie Wu, Ming Li, Tao Yang, Xiaojie Li, Rui Wang, Andrew Bai, Yuanhao Ban, and Cho-Jui Hsieh. Self-forcing++: Towards minute-scale high-quality video generation. *arXiv:2510.02283*, 2025. 2
- [22] Duolikun Danier, Mehmet Aygün, Changjian Li, Hakan Bilen, and Oisín Mac Aodha. Depthcues: Evaluating monocular depth perception in large vision models. In *CVPR*, 2025. 2, 4
- [23] Matt Deitke, Ruoshi Liu, Matthew Wallingford, Huong Ngo, Oscar Michel, Aditya Kusupati, Alan Fan, Christian Laforte, Vikram Voleti, Samir Yitzhak Gadre, et al. Objaverse-xl: A universe of 10m+ 3d objects. *NeurIPS*, 2024. 6
- [24] Haoge Deng, Ting Pan, Haiwen Diao, Zhengxiong Luo, Yufeng Cui, Huchuan Lu, Shiguang Shan, Yonggang Qi, and Xinlong Wang. Autoregressive video generation without vector quantization. *ICLR*, 2025. 2
- [25] Alexey Dosovitskiy, Lucas Beyer, Alexander Kolesnikov, Dirk Weissenborn, Xiaohua Zhai, Thomas Unterthiner, Mostafa Dehghani, Matthias Minderer, Georg Heigold, Sylvain Gelly, Jakob Uszkoreit, and Neil Houlsby. An image is worth 16x16 words: Transformers for image recognition at scale. *ICLR*, 2021. 2
- [26] Haoyi Duan, Hong-Xing Yu, Sirui Chen, Li Fei-Fei, and Jiajun Wu. Worldscore: A unified evaluation benchmark for world generation. *ICCV*, 2025. 3, 7, 18
- [27] Mohamed El Banani, Amit Raj, Kevis-Kokitsi Maninis, Abhishek Kar, Yuanzhen Li, Michael Rubinstein, Deqing Sun, Leonidas Guibas, Justin Johnson, and Varun Jampani. Probing the 3d awareness of visual foundation models. In *CVPR*, 2024. 3, 4, 17

- [28] Stephanie Fu, Mark Hamilton, Laura Brandt, Axel Feldman, Zhoutong Zhang, and William T Freeman. Featup: A model-agnostic framework for features at any resolution. *ICLR*, 2024. 3
- [29] Ruiqi Gao, Aleksander Holynski, Philipp Henzler, Arthur Brussee, Ricardo Martin-Brualla, Pratul Srinivasan, Jonathan T Barron, and Ben Poole. Cat3d: Create anything in 3d with multi-view diffusion models. *NeurIPS*, 2024. 2
- [30] Zekai Gu, Rui Yan, Jiahao Lu, Peng Li, Zhiyang Dou, Chenyang Si, Zhen Dong, Qifeng Liu, Cheng Lin, Ziwei Liu, et al. Diffusion as shader: 3d-aware video diffusion for versatile video generation control. In *SIGGRAPH*, 2025. 1, 2, 3, 17
- [31] Yuwei Guo, Ceyuan Yang, Anyi Rao, Zhengyang Liang, Yaohui Wang, Yu Qiao, Maneesh Agrawala, Dahua Lin, and Bo Dai. Animatediff: Animate your personalized text-to-image diffusion models without specific tuning. *ICLR*, 2024. 1, 2, 8, 17
- [32] Hao He, Yinghao Xu, Yuwei Guo, Gordon Wetzstein, Bo Dai, Hongsheng Li, and Ceyuan Yang. Cameractrl: Enabling camera control for video diffusion models. In *ICLR*, 2025. 1, 2, 3, 5, 6, 7, 8, 16, 17, 18
- [33] Xu He, Qiaochu Huang, Zhensong Zhang, Zhiwei Lin, Zhiyong Wu, Sicheng Yang, Minglei Li, Zhiyi Chen, Songcen Xu, and Xiaofei Wu. Co-speech gesture video generation via motion-decoupled diffusion model. In *CVPR*, 2024. 2
- [34] Yingqing He, Tianyu Yang, Yong Zhang, Ying Shan, and Qifeng Chen. Latent video diffusion models for high-fidelity long video generation. *arXiv:2211.13221*, 2022. 2
- [35] Martin Heusel, Hubert Ramsauer, Thomas Unterthiner, Bernhard Nessler, and Sepp Hochreiter. Gans trained by a two time-scale update rule converge to a local nash equilibrium. *NeurIPS*, 30, 2017. 14
- [36] Jonathan Ho, Ajay Jain, and Pieter Abbeel. Denoising diffusion probabilistic models. *NeurIPS*, 2020. 1, 2, 4
- [37] Jonathan Ho, Tim Salimans, Alexey Gritsenko, William Chan, Mohammad Norouzi, and David J Fleet. Video diffusion models. *NeurIPS*, 2022. 2
- [38] Chen Hou and Zhibo Chen. Training-free camera control for video generation. In *ICLR*, 2025. 2
- [39] Li Hu. Animate anyone: Consistent and controllable image-to-video synthesis for character animation. In *CVPR*, 2024. 2
- [40] Teng Hu, Jiangning Zhang, Ran Yi, Yating Wang, Jieyu Weng, Hongrui Huang, Yabiao Wang, and Lizhuang Ma. Comd: Training-free video motion transfer with camera-object motion disentanglement. In *ACM Multimedia*, 2024. 2
- [41] Chun-Hao Paul Huang, Niloy Mitra, Hyeonho Jeong, Jae Shin Yoon, and Duygu Ceylan. Jog3r: Towards 3d-consistent video generators. *BMVC*, 2025. 1, 2, 3, 4, 5, 6, 7
- [42] Xun Huang, Zhengqi Li, Guande He, Mingyuan Zhou, and Eli Shechtman. Self forcing: Bridging the train-test gap in autoregressive video diffusion. *NeurIPS*, 2025. 2
- [43] Ziqi Huang, Yanan He, Jiashuo Yu, Fan Zhang, Chenyang Si, Yuming Jiang, Yuanhan Zhang, Tianxing Wu, Qingyang Jin, Nattapol Chanpaisit, et al. Vbench: Comprehensive benchmark suite for video generative models. In *CVPR*, 2024. 8
- [44] Sungwon Hwang, Hyojin Jang, Kinam Kim, Minho Park, and Jaegul Choo. Cross-frame representation alignment for fine-tuning video diffusion models. *arXiv:2506.09229*, 2025. 3
- [45] Hyeonho Jeong, Chun-Hao P Huang, Jong Chul Ye, Niloy J Mitra, and Duygu Ceylan. Track4gen: Teaching video diffusion models to track points improves video generation. In *CVPR*, 2025. 1, 2, 4, 5, 6, 7
- [46] Tero Karras, Miika Aittala, Timo Aila, and Samuli Laine. Elucidating the design space of diffusion-based generative models. *NeurIPS*, 2022. 2, 4
- [47] Bernhard Kerbl, Georgios Kopanas, Thomas Leimkühler, and George Drettakis. 3d gaussian splatting for real-time radiance field rendering. *ACM Transactions on Graphics*, 2023. 2
- [48] Weijie Kong, Qi Tian, Zijian Zhang, Rox Min, Zuozhuo Dai, Jin Zhou, Jiangfeng Xiong, Xin Li, Bo Wu, Jianwei Zhang, et al. Hunyuanvideo: A systematic framework for large video generative models. *arXiv:2412.03603*, 2024. 2, 15
- [49] Zhengfei Kuang, Shengqu Cai, Hao He, Yinghao Xu, Hongsheng Li, Leonidas J Guibas, and Gordon Wetzstein. Collaborative video diffusion: Consistent multi-video generation with camera control. *NeurIPS*, 2024. 2
- [50] Xingjian Leng, Jaskirat Singh, Yunzhong Hou, Zhenchang Xing, Saining Xie, and Liang Zheng. Repa-e: Unlocking vae for end-to-end tuning with latent diffusion transformers. *ICCV*, 2025. 1, 2
- [51] Vincent Leroy, Yohann Cabon, and Jérôme Revaud. Grounding image matching in 3d with mast3r. In *ECCV*, 2024. 18
- [52] Teng Li, Guangcong Zheng, Rui Jiang, Shuigen Zhan, Tao Wu, Yehao Lu, Yining Lin, Chuanyun Deng, Yapan Xiong, Min Chen, et al. Realcam-i2v: Real-world image-to-video generation with interactive complex camera control. In *ICCV*, 2025. 2, 3, 7, 8, 17, 18
- [53] Yaowei Li, Xintao Wang, Zhaoyang Zhang, Zhouxia Wang, Ziyang Yuan, Liangbin Xie, Ying Shan, and Yuexian Zou. Image conductor: Precision control for interactive video synthesis. In *AAAI*, 2025. 2
- [54] Ruofan Liang, Zan Gojcic, Huan Ling, Jacob Munkberg, Jon Hasselgren, Chih-Hao Lin, Jun Gao, Alexander Keller, Nandita Vijaykumar, Sanja Fidler, et al. Diffusion renderer: Neural inverse and forward rendering with video diffusion models. In *CVPR*, 2025. 1
- [55] Lu Ling, Yichen Sheng, Zhi Tu, Wentian Zhao, Cheng Xin, Kun Wan, Lantao Yu, Qianyu Guo, Zixun Yu, Yawen Lu, et al. D3dv-10k: A large-scale scene dataset for deep learning-based 3d vision. In *CVPR*, 2024. 3, 5, 6, 16
- [56] Yaron Lipman, Ricky TQ Chen, Heli Ben-Hamu, Maximilian Nickel, and Matt Le. Flow matching for generative modeling. *ICLR*, 2023. 4

- [57] Xinyu Liu, Ailing Zeng, Wei Xue, Harry Yang, Wenhan Luo, Qifeng Liu, and Yike Guo. Vfx creator: Animated visual effect generation with controllable diffusion transformer. *arXiv:2502.05979*, 2025. 1
- [58] Yuan Liu, Cheng Lin, Zijiao Zeng, Xiaoxiao Long, Lingjie Liu, Taku Komura, and Wenping Wang. Syncdreamer: Generating multiview-consistent images from a single-view image. *ICLR*, 2024. 1, 2
- [59] Ilya Loshchilov and Frank Hutter. Decoupled weight decay regularization. *ICLR*, 2019. 17
- [60] Nanye Ma, Mark Goldstein, Michael S Albergo, Nicholas M Boffi, Eric Vanden-Eijnden, and Saining Xie. Sit: Exploring flow and diffusion-based generative models with scalable interpolant transformers. In *ECCV*, 2024. 1
- [61] Wufei Ma, Guofeng Zhang, Qihao Liu, Guanning Zeng, Adam Kortylewski, Yaoyao Liu, and Alan Yuille. Imagenet3d: Towards general-purpose object-level 3d understanding. *NeurIPS*, 2024. 2, 3
- [62] Jinjie Mai, Wenxuan Zhu, Haozhe Liu, Bing Li, Cheng Zheng, Jürgen Schmidhuber, and Bernard Ghanem. Can video diffusion model reconstruct 4d geometry? *arXiv:2503.21082*, 2025. 2
- [63] Yunze Man, Shuhong Zheng, Zhipeng Bao, Martial Hebert, Liang-Yan Gui, and Yu-Xiong Wang. Lexicon3d: Probing visual foundation models for complex 3d scene understanding. In *NeurIPS*, 2024. 2
- [64] Mateusz Michalkiewicz, Sheena Bai, Mahsa Baktashmotlagh, Varun Jampani, and Guha Balakrishnan. Not all views are created equal: Analyzing viewpoint instabilities in vision foundation models. In *CVPR*, 2025. 2, 3
- [65] Ben Mildenhall, Pratul P Srinivasan, Matthew Tancik, Jonathan T Barron, Ravi Ramamoorthi, and Ren Ng. Nerf: Representing scenes as neural radiance fields for view synthesis. *Communications of the ACM*, 2021. 2
- [66] Thomas Mitchel, Michael J Taylor, and Vincent Sitzmann. Neural isometries: Taming transformations for equivariant ml. *NeurIPS*, 2024. 4
- [67] Kepan Nan, Rui Xie, Penghao Zhou, Tiehan Fan, Zhenheng Yang, Zhijie Chen, Xiang Li, Jian Yang, and Ying Tai. Openvid-1m: A large-scale high-quality dataset for text-to-video generation. *ICLR*, 2025. 2
- [68] Maxime Oquab, Timothée Darcet, Théo Moutakanni, Huy V. Vo, Marc Szafraniec, Vasil Khalidov, Pierre Fernandez, Daniel HAZIZA, Francisco Massa, Alaaeldin El-Nouby, Mido Assran, Nicolas Ballas, Wojciech Galuba, Russell Howes, Po-Yao Huang, Shang-Wen Li, Ishan Misra, Michael Rabbat, Vasu Sharma, Gabriel Synnaeve, Hu Xu, Herve Jegou, Julien Mairal, Patrick Labatut, Armand Joulin, and Piotr Bojanowski. DINOv2: Learning robust visual features without supervision. *TMLR*, 2024. 1, 3
- [69] Linfei Pan, Daniel Barath, Marc Pollefeys, and Johannes Lutz Schönberger. Global Structure-from-Motion Revisited. In *ECCV*, 2024. 5, 18
- [70] William Peebles and Saining Xie. Scalable diffusion models with transformers. In *ICCV*, 2023. 1, 2, 4, 15
- [71] Xuanchi Ren, Tianchang Shen, Jiahui Huang, Huan Ling, Yifan Lu, Merlin Nimier-David, Thomas Müller, Alexander Keller, Sanja Fidler, and Jun Gao. Gen3c: 3d-informed world-consistent video generation with precise camera control. In *CVPR*, 2025. 1, 2, 3, 7, 8, 17
- [72] Ignacio Rocco, Relja Arandjelovic, and Josef Sivic. Convolutional neural network architecture for geometric matching. In *CVPR*, 2017. 3
- [73] Robin Rombach, Andreas Blattmann, Dominik Lorenz, Patrick Esser, and Björn Ommer. High-resolution image synthesis with latent diffusion models. In *CVPR*, 2022. 1, 2, 4
- [74] Olaf Ronneberger, Philipp Fischer, and Thomas Brox. U-net: Convolutional networks for biomedical image segmentation. In *MICCAI*, 2015. 4
- [75] Tim Salimans and Jonathan Ho. Progressive distillation for fast sampling of diffusion models. *ICLR*, 2022. 4
- [76] Johannes Lutz Schönberger and Jan-Michael Frahm. Structure-from-motion revisited. In *CVPR*, 2016. 5, 7, 18
- [77] Johannes Lutz Schönberger, Enliang Zheng, Marc Pollefeys, and Jan-Michael Frahm. Pixelwise view selection for unstructured multi-view stereo. In *ECCV*, 2016. 5
- [78] Katja Schwarz, Norman Mueller, and Peter Kotschieder. Generative gaussian splatting: Generating 3d scenes with video diffusion priors. *ICCV*, 2025. 1, 2
- [79] Kiwhan Song, Boyuan Chen, Max Simchowitz, Yilun Du, Russ Tedrake, and Vincent Sitzmann. History-guided video diffusion. *ICML*, 2025. 8
- [80] Yang Song, Jascha Sohl-Dickstein, Diederik P Kingma, Abhishek Kumar, Stefano Ermon, and Ben Poole. Score-based generative modeling through stochastic differential equations. *ICLR*, 2021. 4
- [81] Jiaming Sun, Zehong Shen, Yuang Wang, Hujun Bao, and Xiaowei Zhou. Loft: Detector-free local feature matching with transformers. In *CVPR*, 2021. 3, 17
- [82] Stanislaw Szymanowicz, Jason Y Zhang, Pratul Srinivasan, Ruiqi Gao, Arthur Brussee, Aleksander Holynski, Ricardo Martin-Brualla, Jonathan T Barron, and Philipp Henzler. Bolt3d: Generating 3d scenes in seconds. In *ICCV*, 2025. 1, 2, 3
- [83] Jiayang Tang, Zhaoxi Chen, Xiaokang Chen, Tengfei Wang, Gang Zeng, and Ziwei Liu. LGM: Large multi-view gaussian model for high-resolution 3d content creation. In *ECCV*, 2024. 18
- [84] Luming Tang, Menglin Jia, Qianqian Wang, Cheng Perng Phoo, and Bharath Hariharan. Emergent correspondence from image diffusion. *NeurIPS*, 2023. 3
- [85] HunyuanWorld Team, Zhenwei Wang, Yuhao Liu, Junta Wu, Zixiao Gu, Haoyuan Wang, Xuhui Zuo, Tianyu Huang, Wenhuan Li, Sheng Zhang, et al. Hunyuanworld 1.0: Generating immersive, explorable, and interactive 3d worlds from words or pixels. *arXiv:2507.21809*, 2025. 1, 3
- [86] Zachary Teed and Jia Deng. Raft: Recurrent all-pairs field transforms for optical flow. In *ECCV*, 2020. 7, 17
- [87] Nikolaos Tsagkas, Jack Rome, Subramanian Ramamoorthy, Oisín Mac Aodha, and Chris Xiaoxuan Lu. Click to grasp: Zero-shot precise manipulation via visual diffusion descriptors. In *IROS*, 2024. 2

- [88] Narek Tumanyan, Assaf Singer, Shai Bagon, and Tali Dekel. Dino-tracker: Taming dino for self-supervised point tracking in a single video. In *ECCV*, 2024. 4
- [89] Thomas Unterthiner, Sjoerd Van Steenkiste, Karol Kurach, Raphael Marinier, Marcin Michalski, and Sylvain Gelly. Towards accurate generative models of video: A new metric & challenges. *arXiv:1812.01717*, 2018. 7
- [90] Vikram Voleti, Chun-Han Yao, Mark Boss, Adam Letts, David Pankratz, Dmitry Tochilkin, Christian Laforte, Robin Rombach, and Varun Jampani. SV3D: Novel multi-view synthesis and 3d generation from a single image using latent video diffusion. In *ECCV*, 2024. 6, 8, 14, 17
- [91] Team Wan, Ang Wang, Baole Ai, Bin Wen, Chaojie Mao, Chen-Wei Xie, Di Chen, Feiwu Yu, Haiming Zhao, Jianxiao Yang, et al. Wan: Open and advanced large-scale video generative models. *arXiv:2503.20314*, 2025. 2
- [92] Jianyuan Wang, Minghao Chen, Nikita Karaev, Andrea Vedaldi, Christian Rupprecht, and David Novotny. Vggg: Visual geometry grounded transformer. In *CVPR*, 2025. 2, 3, 5, 8, 14
- [93] Ruicheng Wang, Sicheng Xu, Cassie Dai, Jianfeng Xiang, Yu Deng, Xin Tong, and Jiaolong Yang. Moge: Unlocking accurate monocular geometry estimation for open-domain images with optimal training supervision. In *CVPR*, 2025. 17
- [94] Shuzhe Wang, Vincent Leroy, Yohann Cabon, Boris Chidlovskii, and Jerome Revaud. Dust3r: Geometric 3d vision made easy. In *CVPR*, 2024. 2, 8
- [95] Yaohui Wang, Xinyuan Chen, Xin Ma, Shangchen Zhou, Ziqi Huang, Yi Wang, Ceyuan Yang, Yanan He, Jiashuo Yu, Peiqing Yang, et al. Lavie: High-quality video generation with cascaded latent diffusion models. *IJCV*, 2025. 2
- [96] Yimu Wang, Xuye Liu, Wei Pang, Li Ma, Shuai Yuan, Paul Debevec, and Ning Yu. Survey of video diffusion models: Foundations, implementations, and applications. *TMLR*, 2025. 8
- [97] Zhou Wang, Alan C Bovik, Hamid R Sheikh, and Eero P Simoncelli. Image quality assessment: from error visibility to structural similarity. *Transactions on Image Processing*, 2004. 7
- [98] Zhouxia Wang, Ziyang Yuan, Xintao Wang, Yaowei Li, Tianshui Chen, Menghan Xia, Ping Luo, and Ying Shan. Motionctrl: A unified and flexible motion controller for video generation. In *SIGGRAPH*, 2024. 2, 3, 6, 8, 17
- [99] Haoyu Wu, Diankun Wu, Tianyu He, Junliang Guo, Yang Ye, Yueqi Duan, and Jiang Bian. Geometry forcing: Marrying video diffusion and 3d representation for consistent world modeling. *arXiv:2507.07982*, 2025. 1, 2, 3, 4, 7
- [100] Rundi Wu, Ruiqi Gao, Ben Poole, Alex Trevithick, Changxi Zheng, Jonathan T Barron, and Aleksander Holynski. Cat4d: Create anything in 4d with multi-view video diffusion models. In *CVPR*, 2025. 1
- [101] Tong Wu, Jiarui Zhang, Xiao Fu, Yuxin Wang, Jiawei Ren, Liang Pan, Wayne Wu, Lei Yang, Jiaqi Wang, Chen Qian, et al. OmniObject3D: Large-vocabulary 3d object dataset for realistic perception, reconstruction and generation. In *CVPR*, 2023. 6, 14
- [102] Junfei Xiao, Ceyuan Yang, Lvmin Zhang, Shengqu Cai, Yang Zhao, Yuwei Guo, Gordon Wetzstein, Maneesh Agrawala, Alan Yuille, and Lu Jiang. Captain cinema: Towards short movie generation. *arXiv:2507.18634*, 2025. 1
- [103] Xianghui Xie, Chuhang Zou, Meher Gitika Karumuri, Jan Eric Lenssen, and Gerard Pons-Moll. Mvgbench: Comprehensive benchmark for multi-view generation models. *ICCV*, 2025. 1, 2, 4, 6, 7, 8, 14, 17
- [104] Jinbo Xing, Menghan Xia, Yong Zhang, Haoxin Chen, Wangbo Yu, Hanyuan Liu, Gongye Liu, Xintao Wang, Ying Shan, and Tien-Tsin Wong. Dynamicrafter: Animating open-domain images with video diffusion priors. In *ECCV*, 2024. 2
- [105] DeJia Xu, Weili Nie, Chao Liu, Sifei Liu, Jan Kautz, Zhangyang Wang, and Arash Vahdat. Camco: Camera-controllable 3d-consistent image-to-video generation. *arXiv:2406.02509*, 2024. 2
- [106] Lihe Yang, Bingyi Kang, Zilong Huang, Zhen Zhao, Xiaogang Xu, Jiashi Feng, and Hengshuang Zhao. Depth anything v2. *NeurIPS*, 2024. 17
- [107] Shiyuan Yang, Liang Hou, Haibin Huang, Chongyang Ma, Pengfei Wan, Di Zhang, Xiaodong Chen, and Jing Liao. Direct-a-video: Customized video generation with user-directed camera movement and object motion. In *SIGGRAPH*, 2024. 2
- [108] Zhuoran Yang, Xi Guo, Chenjing Ding, Chiyu Wang, Wei Wu, and Yanyong Zhang. Instadrive: Instance-aware driving world models for realistic and consistent video generation. In *ICCV*, 2025. 1
- [109] Zhuoyi Yang, Jiayan Teng, Wendi Zheng, Ming Ding, Shiyu Huang, Jiazheng Xu, Yuanming Yang, Wenyi Hong, Xiaohan Zhang, Guanyu Feng, et al. Cogvideox: Text-to-video diffusion models with an expert transformer. *ICLR*, 2025. 2, 8, 15
- [110] Yang You, Yixin Li, Congyue Deng, Yue Wang, and Leonidas Guibas. Multiview equivariance improves 3d correspondence understanding with minimal feature finetuning. *ICLR*, 2025. 2, 3, 4, 5
- [111] Sihyun Yu, Sangkyung Kwak, Huiwon Jang, Jongheon Jeong, Jonathan Huang, Jinwoo Shin, and Saining Xie. Representation alignment for generation: Training diffusion transformers is easier than you think. *ICLR*, 2025. 1, 2
- [112] Yuanwen Yue, Anurag Das, Francis Engelmann, Siyu Tang, and Jan Eric Lenssen. Improving 2d feature representations by 3d-aware fine-tuning. In *ECCV*, 2024. 2, 3, 4
- [113] Guanqi Zhan, Chuanxia Zheng, Weidi Xie, and Andrew Zisserman. A general protocol to probe large vision models for 3d physical understanding. In *NeurIPS*, 2024. 2
- [114] Junyi Zhang, Charles Herrmann, Junhwa Hur, Luisa Polania Cabrera, Varun Jampani, Deqing Sun, and Ming-Hsuan Yang. A tale of two features: Stable diffusion complements dino for zero-shot semantic correspondence. *NeurIPS*, 2023. 2, 3
- [115] Qihang Zhang, Shuangfei Zhai, Miguel Angel Bautista Martin, Kevin Miao, Alexander Toshev, Joshua Susskind, and Jiatao Gu. World-consistent video diffusion with explicit 3d modeling. In *CVPR*, 2025. 1, 2, 3, 4

- [116] Richard Zhang, Phillip Isola, Alexei A Efros, Eli Shechtman, and Oliver Wang. The unreasonable effectiveness of deep features as a perceptual metric. In *CVPR*, 2018. [7](#)
- [117] Xiangdong Zhang, Jiaqi Liao, Shaofeng Zhang, Fanqing Meng, Xiangpeng Wan, Junchi Yan, and Yu Cheng. Videorepa: Learning physics for video generation through relational alignment with foundation models. *arXiv:2505.23656*, 2025. [1](#), [3](#)
- [118] Yiming Zhang, Zhening Xing, Yanhong Zeng, Youqing Fang, and Kai Chen. Pia: Your personalized image animator via plug-and-play modules in text-to-image models. In *CVPR*, 2024. [2](#)
- [119] Min Zhao, Guande He, Yixiao Chen, Hongzhou Zhu, Chongxuan Li, and Jun Zhu. Riflex: A free lunch for length extrapolation in video diffusion transformers. *ICML*, 2025. [2](#)
- [120] Dian Zheng, Ziqi Huang, Hongbo Liu, Kai Zou, Yinan He, Fan Zhang, Lulu Gu, Yuanhan Zhang, Jingwen He, Wei-Shi Zheng, et al. Vbench-2.0: Advancing video generation benchmark suite for intrinsic faithfulness. *arXiv:2503.21755*, 2025. [1](#)
- [121] Zangwei Zheng, Xiangyu Peng, Tianji Yang, Chenhui Shen, Shenggui Li, Hongxin Liu, Yukun Zhou, Tianyi Li, and Yang You. Open-sora: Democratizing efficient video production for all. *arXiv:2412.20404*, 2024. [2](#)
- [122] Chaoyi Zhou, Xi Liu, Feng Luo, and Siyu Huang. Latent radiance fields with 3d-aware 2d representations. In *ICLR*, 2025. [3](#)
- [123] Tinghui Zhou, Richard Tucker, John Flynn, Graham Fyffe, and Noah Snavely. Stereo magnification: Learning view synthesis using multiplane images. *SIGGRAPH*, 2018. [3](#), [5](#), [6](#), [16](#)

# Appendix

We provide additional materials to supplement our main paper. In Sec. A we provide additional experiment results including a user study, complementary quantitative and qualitative evaluations, as well as discussion on limitations and failure cases of our method. In Sec. B, we provide additional details for the 3D consistency analysis, and specify further implementation details on training and evaluation of video generation models.

## A. Additional results

### A.1. User study

In order to further validate the perceptual improvement in 3D consistency brought by ViCoDR, we performed a user study. We adopted the two-alternative forced choice (2AFC) approach to compare CameraCtrl trained with our method (Ours) against each of four baselines: CameraCtrl (the default setting); CameraCtrl trained with JOG3R, GF, or Track4Gen. In each comparison (*i.e.*, Ours vs. one of the baselines), the participant was shown pairs of videos, where within each pair, one video was generated by our method and the other by a baseline method provided with identical input. The spatial presentation ordering of the two videos was randomized. The test videos were sampled from the RE10K and DL3DV test sets after filtering out videos with insufficient camera movement, *i.e.*, ones in which the baseline between the first and last frames was less than 10% of the median scene depth, where the poses and depth are obtained with VGGT [92]. Participants were asked to choose a video to answer the question “Which video keeps shapes and structures more consistent?”. A total of 53 participants completed the survey. Ethics approval for our study was obtained approval from our relevant internal Institutional Review Board.

The user study results are summarized in Fig. A1, where we report the mean and standard deviation of preference ratios for each method across sequences. We observe that our method significantly outperformed all the baselines in maintaining 3D consistency. The user study results are aligned with the quantitative metrics, and further confirms the effectiveness of ViCoDR.

### A.2. Additional quantitative results

**MotionCtrl.** In the main paper, we reported the average results of ViCoDR on MotionCtrl over three runs with different seeds. In Tab. A1 we additionally report the standard deviations for completeness, where we observe reasonably small magnitudes.

**ViFiGen.** In addition to the MVGBench metrics reported in the main paper, we also compute conventional image-level reconstruction metrics on OmniObject3D [101] in Tab. A2.

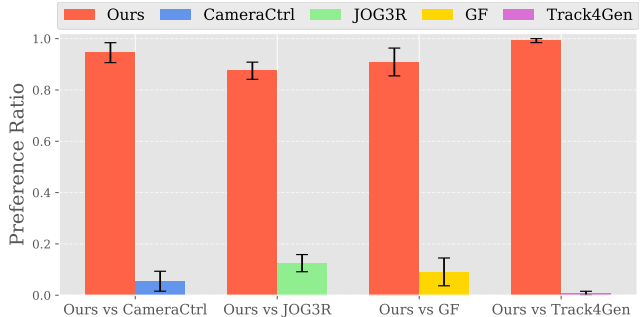


Figure A1. **User study results.** Preference ratio of each method is plotted in four sets of comparisons. Our method significantly outperforms all baselines.

The OmniObject3D dataset contains 6,000 scanned objects across 190 common object categories. We render 21 target views for each test object and compare each generated image with its corresponding ground-truth view. We report mean PSNR (mPSNR), mean SSIM (mSSIM), and mean LPIPS (mLPIPS) by first averaging over views for each object and then averaging over all objects. For FID, we follow the standard protocol and compute the Fréchet Inception Distance (FID) [35] between the distribution of generated views and the corresponding ground-truth views. Note that this evaluation differs from the 3DGS-based self-consistency metrics of MVGBench [103], and is closer in spirit to the GT-based multi-view evaluation used in SV3D [90]. For fairness, the ViFiGen baseline is trained on the same data and setup as our method, as further detailed in Sec. B.2. As shown in Tab. A2, our approach consistently outperforms ViFiGen across all metrics, corroborating the gains demonstrated in the main paper.

### A.3. Additional qualitative results

Here we provide additional qualitative results of applying ViCoDR to the three base models: CameraCtrl (Fig. A7, Fig. A8), MotionCtrl (Fig. A9), and ViFiGen (Fig. A6). A **supplementary video** is also provided. It can be observed from these results that ViCoDR better preserves object shape and texture across multiple views compared to the baselines.

### A.4. Limitations and failure cases

In addition to the limitations discussed in the main paper (see Sec. 5.5), here we expand on the limitations of ViCoDR in terms of performance and additional training cost.

**Failure case 1.** It is observed that, under the same training iterations, although the base models trained with ViCoDR show improved 3D consistency compared to when they are trained without ViCoDR (supported by both quantitative and qualitative evaluation), they can still produce visual artifacts. Fig. A2 shows an example of this, where

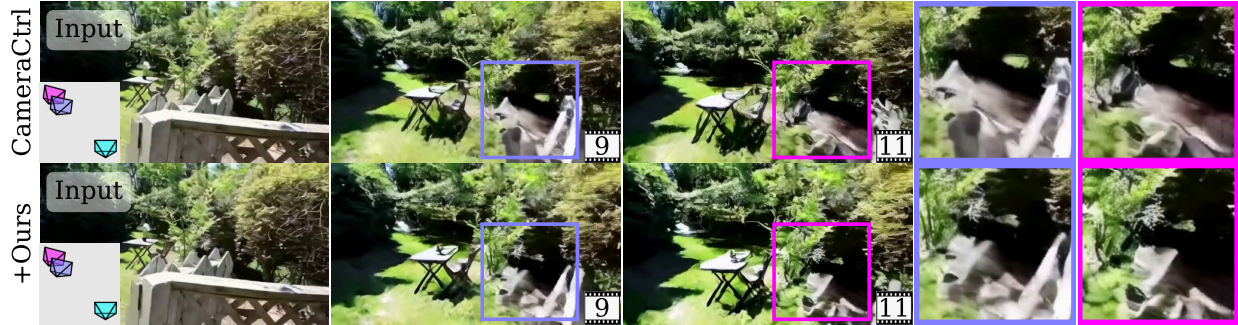


Figure A2. **Failure case 1: very large view changes.** Given the **input frame**, ViCoDR fails to improve the 3D consistency of CameraCtrl in the highlighted region across **view one** and **view two**, which is exposed to large view changes. ViCoDR produces clearer edges.

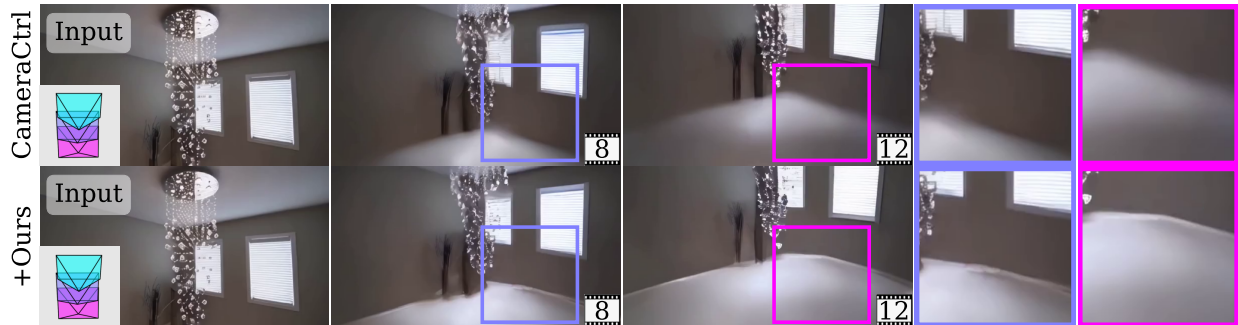


Figure A3. **Failure case 2: clearer but distorted edges.** Given the **input frame**, compared to CameraCtrl, ViCoDR produces clearer edges across **view one** and **view two**. However, this can appear less natural compared to the smeared edges in the CameraCtrl output.

Table A1. **Results of ViCoDR on text-to-video generation.** ViCoDR improves MotionCtrl in terms of **video quality**, **camera control**, and **3D consistency** metrics. Mean and standard deviation over three seeds are reported on RE10K.

Model	FVD (↓)	RotErr (↓)	TransErr (↓)	Succ % (↑)	MEI3R (↓)	RPE (↓)
MotionCtrl	780 (18)	<b>1.119 (0.057)</b>	<b>4.676 (0.238)</b>	89.1 (1.7)	0.075 (0.001)	0.306 (0.008)
+ ViCoDR	<b>559 (14)</b>	1.217 (0.024)	5.288 (0.049)	<b>96.4 (1.1)</b>	<b>0.059 (0.001)</b>	<b>0.255 (0.002)</b>

Table A2. **Additional results on multi-view generation.** On OmniObject3D, ViCoDR effectively and consistently outperforms the baseline ViFiGen, further confirming and aligning with the findings reported in the main text.

Model	mPSNR (↑)	mSSIM (↑)	mLPIPS (↓)	FID (↓)
ViFiGen	19.08	0.77	0.19	27.87
+ ViCoDR	<b>19.78</b>	<b>0.81</b>	<b>0.13</b>	<b>20.35</b>

ViCoDR fails to improve the 3D consistency of CameraCtrl in the fence area across large view changes. As discussed in the main paper, this can be partially due to the inherent limitations of the base model. Specifically, CameraCtrl is based on Stable Video Diffusion, which employs a mostly convolutional U-Net architecture, which can be weaker in capturing long-term spatio-temporal dependencies compared to larger, fully transformer-based architectures [70]. We leave it as future work to explore integrating ViCoDR with such

larger models [48, 109].

**Failure case 2.** As can be seen from the qualitative examples (Sec. A.3), ViCoDR generally preserves edges more clearly compared to the baseline CameraCtrl (likely due to our edge-aware sampling strategy during training, see Sec. A.5). While this is often perceived as improved 3D consistency, in some cases this can lead to lower perceptual quality of the video. This is illustrated in the example in Fig. A3, where our method generates sharper and clearer edges at the corner of the walls compared to the base model. However, these lines appear to violate linear perspective and are not perfectly straight. In contrast, the slightly blurry shadows generated by the baseline CameraCtrl look more natural and can be perceived as being of higher quality. This indicates failed attempts to improve 3D consistency in video generation can even undermine the perceptual quality. An interesting avenue for future research is to study the effect of improved 3D consistency on perceptual quality in video generation.

**Additional training cost.** Training a video generation model with ViCoDR requires additional computation on top of the default diffusion training cost, mainly resulting from the use of VGGT to obtain correspondence labels for  $\mathcal{L}_{3DC}$  (Eq. (5) in the main paper) and the computation of  $\mathcal{L}_{3DC}$  itself. On our hardware setup (detailed in Sec. B.2), this

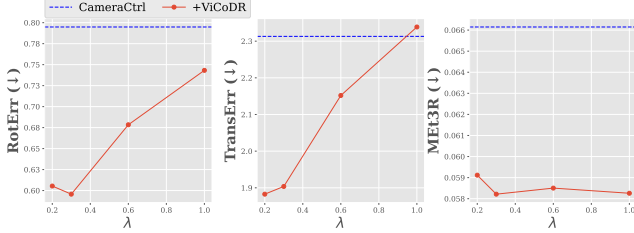


Figure A4. **Impact of  $\lambda$  on RE10K performance.** There exists a trade-off between 3D consistency and camera control accuracy, though ViCoDR still leads to an overall performance improvement.

results in a 23% increase in training time for CameraCtrl, extending 42-hour training time of CameraCtrl to 51 hours.

### A.5. Additional ablation results

**Weight of  $\mathcal{L}_{3DC}$ .** The impact of  $\mathcal{L}_{3DC}$  on the 3D consistency and camera control accuracy of CameraCtrl is discussed in the main paper. Here we provide full evaluation results of models trained with different values of  $\lambda$  (*i.e.*, the weight of  $\mathcal{L}_{3DC}$  in Eq. (4) in the main paper), on RE10K. These results are summarized in Fig. A4, where we observe that even a small value of  $\lambda$  (minimum tested was 0.1) results in a large improvement in 3D consistency (MEt3R), while increasing  $\lambda$  trades off camera control preciseness for small improvements in MEt3R.

**Edge-aware sampling.** When training ViCoDR, we bias the sampling of keypoints towards edges in images (see main paper Sec. 4.3). This design choice is ablated quantitatively in the main paper, and here we provide a qualitative result in Fig. A5 illustrating its effectiveness. We observe that edge-aware sampling results in reduced artifacts on edges, which is also illustrated by the MEt3R [2] reprojection error map.

### A.6. Additional 3D consistency analysis results

In Sec. 3 in the main paper we analyzed seven pre-trained video diffusion models (VDMs) in terms of the 3D consistency of their output videos and their internal diffusion representations. Here we add CameraCtrl trained with ViCoDR (*i.e.*, CameraCtrl+ViCoDR) to this analysis and present the results in Tab. A3. We can see that compared to CameraCtrl re-trained from scratch (initializing with Stable Video Diffusion [7]) with the default settings from the original paper [32] for the same number of iterations (the second row), CameraCtrl+ViCoDR improves both 3D consistency (MEt3R) and geometric correspondence, indicating that more view-consistent representations are effectively learned. Compared to the original pre-trained CameraCtrl, our model achieves better 3D consistency, despite a fourfold reduction in batch size.

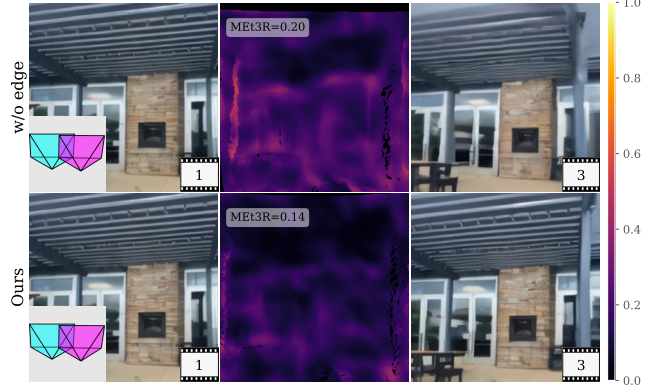


Figure A5. **Visual comparison of removing edge sampling.** Over-sampling keypoints for  $\mathcal{L}_{3DC}$  on edges during training leads to fewer artifacts on lines and corners, as can be seen from the MEt3R reprojection error map (middle column).

Table A3. **Results on 3D consistency and Geometric Correspondence for CameraCtrl trained with and without ViCoDR.** † denotes the pre-trained checkpoint provided in [32].

Model	RE10K		DL3DV	
	MEt3R (↓)	Geo. Corresp. (†)	MEt3R (↓)	Geo. Corresp. (†)
CameraCtrl†	0.060	65.2	0.113	43.8
CameraCtrl	0.066	57.7	0.116	36.7
CameraCtrl+ViCoDR	<b>0.059</b>	<b>91.0</b>	<b>0.110</b>	<b>75.0</b>

## B. Additional implementation details

### B.1. Analysis of 3D consistency experiments

**Datasets.** For the analysis of camera-controlled video diffusion models (VDMs) in Sec. 3 in the main paper, we used RE10K [123] and DL3DV [55] as evaluation datasets. RE10K contains high-quality indoor and outdoor scenes and diverse camera trajectories [32]. As the camera poses in RE10K are mostly smooth, we also report performance on DL3DV [55] which contains more outdoor scenes with more complex poses. Both are commonly used for camera-controlled video generation. We randomly sampled 300 test videos from each for our analysis.

**Models.** Tab. A4 summarizes the versions of the models used in our analysis. When running each model, we follow the official evaluation code and configurations. GEN3C, GWTF, MVGenMaster, DaS, and RealCamI2V require predicting a point cloud from the conditioning input image using an off-the-shelf depth estimation model, and projecting the point cloud to the desired target views. For GWTF, optical flow needs to be extracted from the re-projected frames to warp the input to the diffusion model. We use the external models specified in the original papers or official implementations of the VDMs in our analysis, and note the versions in Tab. A4. Predicting point clouds using a depth model and projecting the point cloud to the desired views

Table A4. **Details of the pre-trained VDMs analyzed for 3D consistency.** The last column specifies the depth/optical flow models used during inference of each model.

Model	Version / Checkpoint	External Models
MVGenMaster [13]	<a href="https://github.com/ewrfcas/MVGenMaster">https://github.com/ewrfcas/MVGenMaster</a>	DepthPro [9]
MotionCtrl [98]	<a href="https://github.com/TencentARC/MotionCtrl/tree/svd">https://github.com/TencentARC/MotionCtrl/tree/svd</a> (CMCM only)	N/A
CameraCtrl [32]	<a href="https://github.com/hehao13/CameraCtrl/tree/svd">https://github.com/hehao13/CameraCtrl/tree/svd</a>	N/A
GWTF [12]	<a href="https://github.com/Eyeline-Labs/Go-with-the-Flow">https://github.com/Eyeline-Labs/Go-with-the-Flow</a>	MoGe [93], RAFT [86]
DaS [30]	<a href="https://github.com/IGL-HKUST/DiffusionAsShader">https://github.com/IGL-HKUST/DiffusionAsShader</a>	MoGe [93]
GEN3C [71]	<a href="https://github.com/nv-tlabs/GEN3C">https://github.com/nv-tlabs/GEN3C</a>	MoGe [93]
RealCamI2V [52]	<a href="https://github.com/ZGCTroy/RealCam-I2V">https://github.com/ZGCTroy/RealCam-I2V</a>	DepthAnythingV2 [106]

requires that the depth prediction and input camera translations are aligned in scale. Therefore, we also run the alignment methods specified in the original papers of the evaluated VDMs to obtain alignment parameters. For GWTF we use the same alignment parameters as GEN3C, as the former does not specify an alignment procedure. We refer the readers to the original papers for more details.

The length of videos output by different models can vary from 14 (CameraCtrl) to 121 (GEN3C) frames. During inference, these VDMs require the same number of input camera poses as the number of frames to generate. Since a 14-frame VDM cannot generate more frames, but it is possible to obtain fewer frames from a VDM that generates more than 14 frames, we limit the evaluated videos and diffusion representations to 14 frames. That is, each test instance consists of an input image and a camera trajectory of length 14. To evaluate a VDM that natively generates more frames than the available sequence length (*e.g.*, GEN3C), we pad the input camera trajectory by repeating the final camera pose in the sequence. At inference time, we retain only the generated frames/diffusion representations corresponding to the first 14 camera poses. Qualitatively we observe no noticeable impact from such padding on the generation quality of the initial 14 frames.

**Geometric Correspondence Evaluation.** To evaluate the multi-view consistency of diffusion representations within each VDM, we evaluated their internal features on the keypoint-free correspondence estimation task [81], as specified in Sec. 3 of the main paper. To extract features from the VDMs, a small amount of noise, which is equivalent to the 1/1000 of the respective highest noise levels, was added to the clean video latents from the VAE encoders. We performed a layer search on each model in an attempt to find the most view-consistent feature encoding layer within each diffusion model. Specifically, we followed [27] and divided the models into four blocks equally, evaluating the features at the end of each block. The performance of the best-performing block was then reported. In terms of the evaluation metric for geometric correspondence, considering the low resolution of the feature maps from VDMs (downsampled by a factor of eight from image resolution

due to VAE encoding, with possibly additional downsampling within the diffusion model depending on the specific architecture), we calculate the pixel-space correspondence recall with a threshold of 50 pixels.

## B.2. ViCoDR training

When training the baseline models CameraCtrl, MotionCtrl, and ViFiGen with ViCoDR, in addition to the hyperparameters specified in the main paper (Sec. 5.1), we set the threshold values for sampling positive and negative samples in  $\mathcal{L}_{3DC}$  (see Sec. 4.3 of main paper) to  $t_{\text{pos}} = 0.005$  and  $t_{\text{neg}} = 0.1$ . Below we specify other hyperparameters and setup details specific to each base model.

**CameraCtrl+ViCoDR.** Both the baseline CameraCtrl and CameraCtrl+ViCoDR are trained following the official training setup in [32], where the VDM is initialized with pre-trained SVD weights [7]. We use the original training dataset, RE10K, provided in [32], where the training videos consist of 14 frames at a resolution of  $576 \times 320$ . Both models are trained with the AdamW optimizer [59] using a learning rate of  $3 \times 10^{-5}$ . Due to computational constraints, we could not match the original batch size of 32 in [32], and use a batch size of eight, achieved via gradient accumulation over two backward passes. The models were trained for 50K iterations (*i.e.*, number of updates). The setup for CameraCtrl+JOG3R/GF/Track4Gen is the same as above. All models were trained on two Nvidia H200 GPUs.

**MotionCtrl+ViCoDR.** We experiment with the AnimateDiff [31]-based version of MotionCtrl, in order to perform text-to-video generation. Following the original setup, both MotionCtrl and MotionCtrl+ViCoDR are trained on RE10K (using captions provided in [32]). The models are initialized with AnimateDiff [31], and trained for 50K iterations with AdamW using a learning rate of  $3 \times 10^{-5}$  with a batch size of eight (again achieved with two gradient accumulation steps), on two H200 GPUs.

**ViFiGen+ViCoDR.** In accordance with the original training protocol [103], both the baseline ViFiGen and our ViFiGen+ViCoDR models are fine-tuned from the pre-trained SV3D backbone [90] using a curated 100k subset of “kiui objects”, obtained from the original Objaverse dataset via

Table A5. **RotErr and TransErr results of ViCoDR on image-to-video generation.** Results are reported only on successfully reconstructed videos common to all methods.

Model	RE10K		DL3DV	
	RotErr ( $\downarrow$ )	TransErr ( $\downarrow$ )	RotErr ( $\downarrow$ )	TransErr ( $\downarrow$ )
CameraCtrl	0.381	1.260	<b>0.725</b>	1.403
+ Track4Gen	0.498	1.945	1.120	1.878
+ GF	0.385	1.322	0.811	1.634
+ JOG3R	0.538	1.786	1.080	1.761
+ ViCoDR (ours)	<b>0.302</b>	<b>1.247</b>	0.773	<b>1.367</b>

Table A6. **RotErr and TransErr results of ViCoDR on text-to-video generation.** Results are reported only on successfully reconstructed videos common to all methods. Mean and standard deviation over three seeds are reported on RE10K.

Model	RotErr ( $\downarrow$ )	TransErr ( $\downarrow$ )
MotionCtrl	0.718 (0.017)	3.509 (0.121)
+ ViCoDR	0.965 (0.039)	4.917 (0.064)

the LGM filtering pipeline [83]. This reduced 100k subset (compared to the original 150k used in ViFiGen) reflects our computational constraints. As in ViFiGen, each object is rendered into 84 views, and then 21 views are randomly sampled per iteration using dynamic-orbit perturbations around a fixed camera ring. Both models share identical optimization hyperparameters so that performance differences can be attributed solely to our view-consistency supervision. We use the official ViFiGen training setup with a reduced batch size. Specifically, AdamW with a learning rate of  $2 \times 10^{-5}$ , batch size four, and 100k training steps on two H200 GPUs. The ViFiGen+ViCoDR variant additionally incorporates the 3D correspondence loss  $\mathcal{L}_{3DC}$  in addition to the standard diffusion objective.

### B.3. Evaluation metrics

To evaluate the *3D consistency* of generated videos, we adopted two established metrics: MET3R [2] and RPE [26]. These measure reprojection error after 3D reconstructing generated videos (RPE uses GLOMAP [69], while MET3R uses MAST3R [51]) in feature space (MET3R) and pixel space (RPE). The intuition behind both of these metrics is that a more 3D-consistent video will result in more accurate 3D reconstruction and keypoint matching, hence leading to smaller reprojection errors. *Camera controllability* was evaluated using Rotation (RotErr) and Translation (TransErr) Errors following [32, 52], which compares the camera poses from the generated video, reconstructed using COLMAP [76], to the input camera trajectory. Note the choice of COLMAP or GLOMAP in these metrics follow the original implementations.

Since SfM can fail on low-quality videos, or videos with insufficient camera baselines (which are rare), we apply a penalty value for RotErr and TransErr to penalize failed re-



Figure A6. **Additional results on multi-view generation.** The red circles highlight regions of improved 3D consistency.

constructions and additionally report the reconstruction success rate (Succ %) of each method. For quantitative comparison on each test set, the penalty value for a metric (*i.e.*, RotErr or TransErr) was set to the 99th percentile of all scores obtained by all models for that metric on that test set. Specifically, in Tab. 1 of the main paper, the penalty values were 3.3 (RE10K) and 4.3 (DL3DV) for RotErr, and 8.0 (RE10K) and 10.0 (DL3DV) for TransErr. In Tab. 2 of the main paper, the penalty values were 4.4 for RotErr and 13.8 for TransErr. In Tab. A5 and Tab. A6 we additionally report RotErr and TransErr considering only common successfully reconstructed sequences between tested models. These results are consistent with our findings in the main paper (see Tab. 1 and Tab. 2).

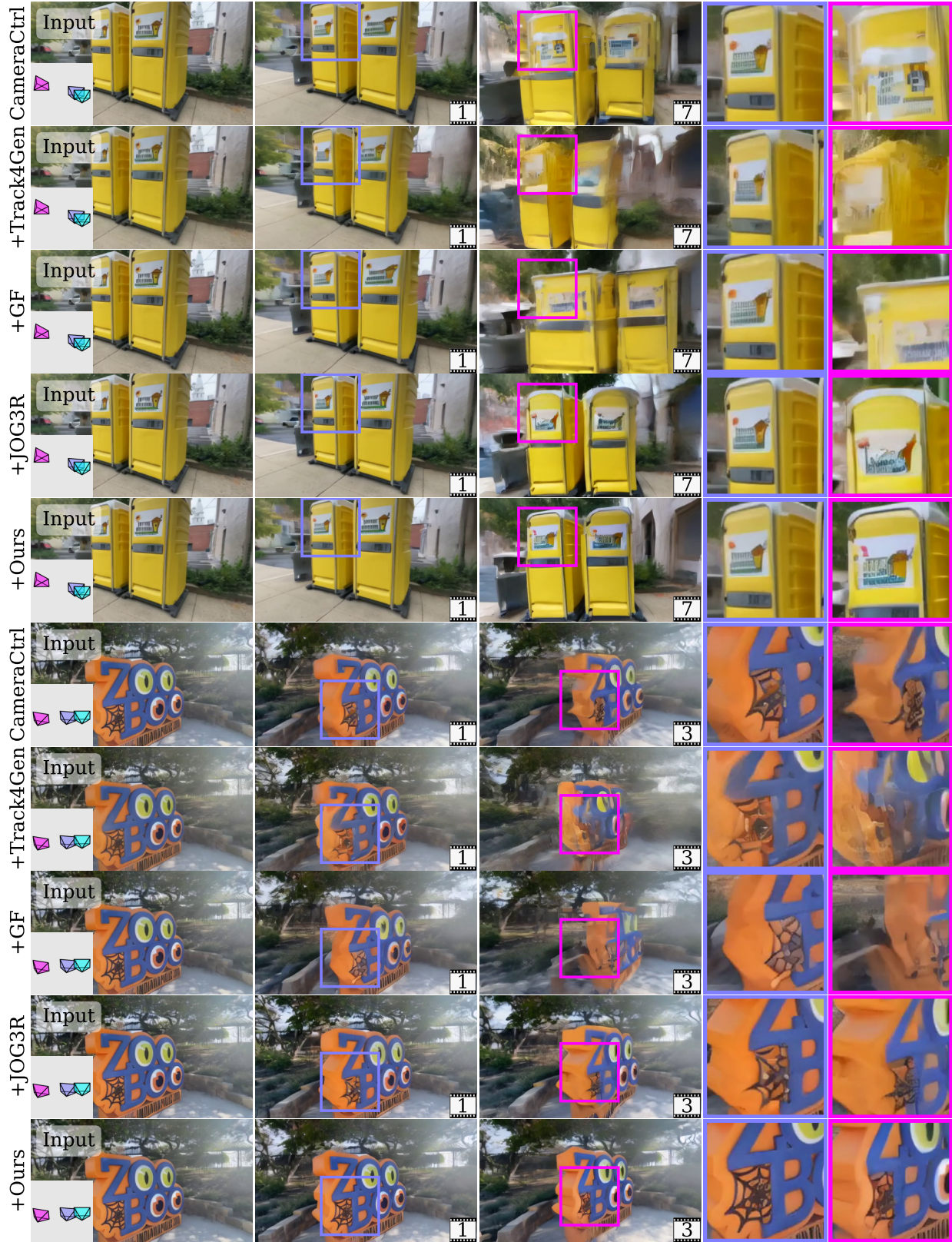


Figure A7. **Additional qualitative results on camera controlled image-to-video generation.** Given the **input frame**, ViCoDR better maintains 3D consistency across **view one** and **view two** compared to the baselines.

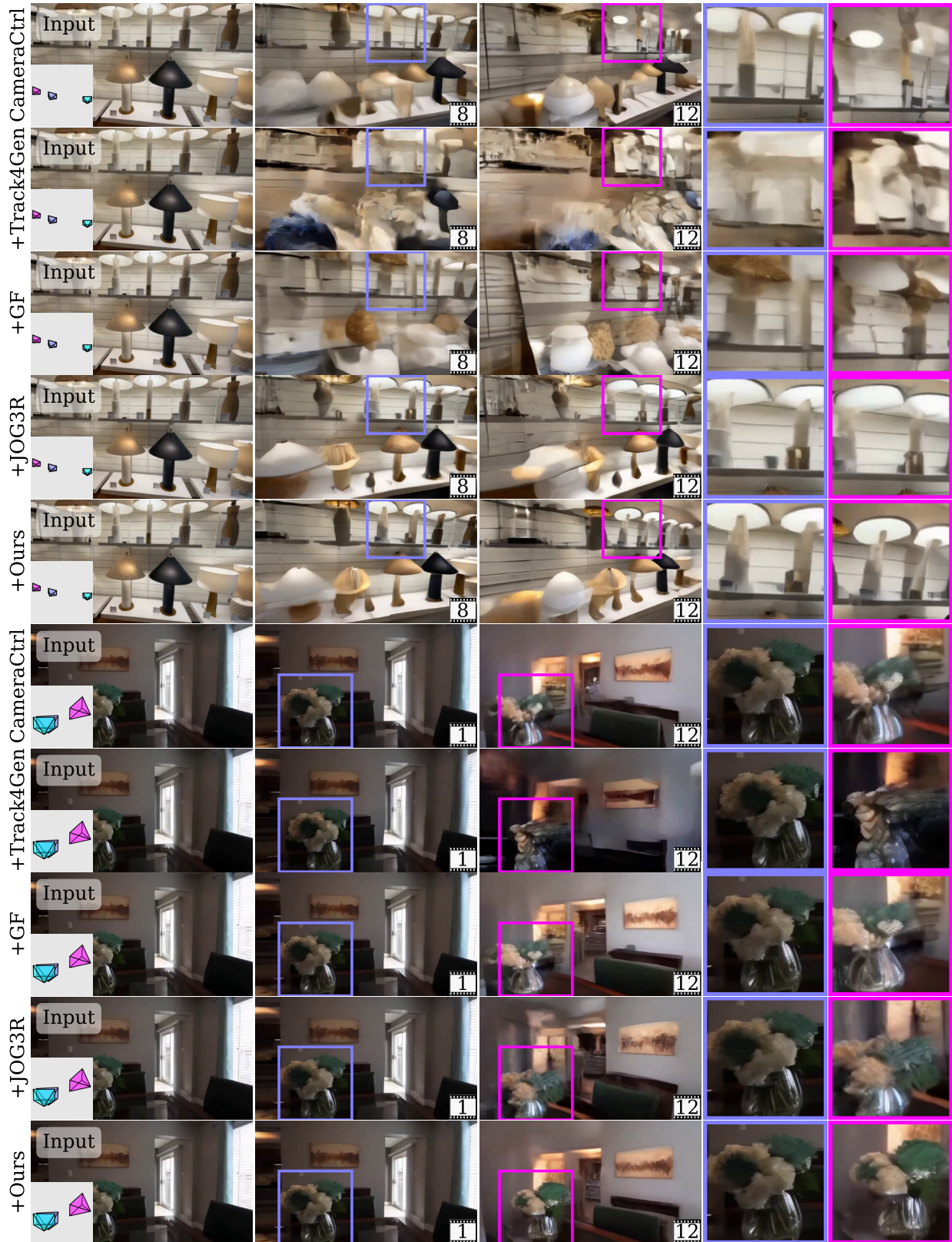


Figure A8. **Additional qualitative results on camera controlled image-to-video generation.** Given the **input frame**, ViCoDR better maintains 3D consistency across **view one** and **view two** compared to the baselines.



Figure A9. **Qualitative results of applying ViCoDR to text-to-video generation.** The input text prompt is shown above the images. Arrows highlight 3D consistent/inconsistent regions.